The Astrophysical Journal, 764:45 (25pp), 2013 February 10 doi:10.1088/0004-637X/764/1/45


# THE DEMOGRAPHICS OF BROAD-LINE QUASARS IN THE MASS–LUMINOSITY PLANE. II. BLACK HOLE MASS AND EDDINGTON RATIO FUNCTIONS

Brandon C. Kelly[1] and Yue Shen[2]
[1] Department of Physics, Broida Hall, University of California, Santa Barbara, CA 93107, USA
[2] Harvard-Smithsonian Center for Astrophysics, 60 Garden Street, MS-51, Cambridge, MA 02138, USA
*Received 2012 September 3; accepted 2012 December 12; published 2013 January 24*

## ABSTRACT

We employ a flexible Bayesian technique to estimate the black hole (BH) mass and Eddington ratio functions for Type 1 (i.e., broad line) quasars from a uniformly selected data set of ∼58,000 quasars from the Sloan Digital Sky Survey (SDSS) DR7. We find that the SDSS becomes significantly incomplete at $M_{\rm BH} \lesssim 3 \times 10^8\,M_\odot$ or $L/L_{\rm Edd} \lesssim 0.07$, and that the number densities of Type 1 quasars continue to increase down to these limits. Both the mass and Eddington ratio functions show evidence of downsizing, with the most massive and highest Eddington ratio BHs experiencing Type 1 quasar phases first, although the Eddington ratio number densities are flat at $z < 2$. We estimate the maximum Eddington ratio of Type 1 quasars in the observable universe to be $L/L_{\rm Edd} \sim 3$. Consistent with our results in Shen & Kelly, we do not find statistical evidence for a so-called sub-Eddington boundary in the mass–luminosity plane of broad-line quasars, and demonstrate that such an apparent boundary in the observed distribution can be caused by selection effect and errors in virial BH mass estimates. Based on the typical Eddington ratio in a given mass bin, we estimate growth times for the BHs in Type 1 quasars and find that they are comparable to or longer than the age of the universe, implying an earlier phase of accelerated (i.e., with higher Eddington ratios) and possibly obscured growth. The large masses probed by our sample imply that most of our BHs reside in what are locally early-type galaxies, and we interpret our results within the context of models of self-regulated BH growth.

*Key words:* black hole physics – galaxies: active – quasars: general – surveys

*Online-only material:* color figures, machine-readable tables

## 1. INTRODUCTION

### 1.1. Background and Motivation

Understanding how and when supermassive black holes (SMBHs) grow is currently one of the great outstanding problems in extragalactic astronomy. The evolution of the galaxy and SMBH populations are not independent, as implied by established correlations between the mass of the SMBH, $M_{\rm BH}$, and properties of the host galaxy bulge, such as luminosity (Kormendy & Richstone 1995; McLure & Dunlop 2001, 2002), stellar velocity dispersion (the $M_{\rm BH}$–$\sigma_*$ relationship, e.g., Gebhardt et al. 2000; Merritt & Ferrarese 2001; Tremaine et al. 2002), concentration or Sérsic index (Graham et al. 2001; Graham & Driver 2007), bulge mass (Magorrian et al. 1998; Marconi & Hunt 2003; Häring & Rix 2004), and binding energy (Aller & Richstone 2007; Hopkins et al. 2007a). Motivated by these empirical trends, a number of authors have invoked active galactic nucleus (AGN[3]) feedback as a means of regulating the SMBH's growth, which ties $M_{\rm BH}$ to properties of the host galaxy (e.g., Silk & Rees 1998; Fabian 1999; Begelman & Nath 2005; Murray et al. 2005; Di Matteo et al. 2005; Springel et al. 2005; Hopkins et al. 2006a; Johansson et al. 2009). In addition to regulating the growth of SMBHs, AGN feedback has been invoked as a means of quenching the growth of the most massive galaxies (e.g., Bower et al. 2006; Croton et al. 2006). Alternatively, it has been suggested that the origin of the scaling relationships emerges from the stochastic nature of the hierarchical assembly of black hole and stellar mass through galaxy mergers (Peng 2007; Jahnke & Macciò 2011). In addition, more recent observational results have painted a more complicated picture, and it is unclear to what degree the scaling relationships between the host galaxy and $M_{\rm BH}$ extend beyond classical bulges or down to lower black hole masses (e.g., Hu 2008; Graham 2008, 2012; Gültekin et al. 2009; Greene et al. 2010b; Jiang et al. 2011; Kormendy et al. 2011).

The galaxy and SMBH populations are also coupled because the fueling of SMBHs, which initiates AGN activity, depends on events that occur within and to the host galaxy. Many models have invoked major mergers of two gas-rich galaxies as the triggering mechanism for quasar activity that provides the bulk of SMBH growth (e.g., Sanders et al. 1988; Sanders & Mirabel 1996; Kauffmann & Haehnelt 2000; Wyithe & Loeb 2003; Springel et al. 2005; Di Matteo et al. 2005; Sijacki et al. 2007; Di Matteo et al. 2008; Hopkins et al. 2008; Somerville et al. 2008; Shen 2009). Models have also invoked large-scale secular instabilities as a means of fueling AGN activity and growing SMBHs in disks (e.g., Bower et al. 2006; Bournaud et al. 2011; Fanidakis et al. 2011). At lower luminosities or redshifts, other fueling mechanisms may dominate the triggering of AGN activity (e.g., Hopkins & Hernquist 2009), such as external interactions (e.g., Serber et al. 2006; Alonso et al. 2007; Woods & Geller 2007; Silverman et al. 2011; Ellison et al. 2011; Liu et al. 2012), stochastic accretion of gas (e.g., Hopkins & Hernquist 2006), bar instabilities (e.g., Shlosman et al. 1989; García-Burillo et al. 2005; Hopkins & Quataert 2010), or stellar mass loss (e.g., Norman & Scoville 1988; Ciotti & Ostriker 1997, 2007; Kauffmann & Heckman 2009; Ho 2009). Regardless of the fueling mechanism, if the SMBH's growth is self-regulated via AGN feedback then the final mass of the SMBH after a fueling event is set by the binding energy of the bulge (Younger et al. 2008).

[3] In this work we will use the terms AGN and quasar to refer to the same type of object. No luminosity difference is implied except where explicitly stated.

Ideally, in order to constrain models of SMBH fueling, growth, and impact on the host galaxy, one would like to follow across time the stochastic process that is the evolution of SMBHs and their hosts. However, this is not possible, so demographic studies must be used to reconstruct the evolution of these populations. Because of this, the demographics of SMBHs, AGNs, and their host galaxies is one of the primary empirical tools that we have for placing constraints on astrophysical models of SMBH growth and fueling. Traditionally, studies of AGN demographics have focused on the luminosity function (e.g., for some recent estimates see Boyle et al. 2000; Fan et al. 2001; Ueda et al. 2003; Wolf et al. 2003; Fan et al. 2004; Barger et al. 2005; Hasinger et al. 2005; Richards et al. 2005, 2006; Fontanot et al. 2007; Bongiorno et al. 2007; Hopkins et al. 2007b; Silverman et al. 2008; Croom et al. 2009; Jiang et al. 2009; Aird et al. 2010; Willott et al. 2010; Fiore et al. 2012; Shen & Kelly 2012). Many recent luminosity function studies lead to the important discovery that the comoving number densities of more luminous AGNs peak at earlier times than do the number densities of less luminous AGNs (e.g., Cowie et al. 2003; Steffen et al. 2003; Ueda et al. 2003; Hasinger et al. 2005; Bongiorno et al. 2007; Croom et al. 2009; Rigby et al. 2011), a phenomenon termed "cosmic downsizing." That the more luminous AGN population turns-off at earlier cosmic epochs implies that the more massive SMBHs grow first.

The luminosity function is the convolution of the black hole mass function (BHMF) with the Eddington ratio distribution, weighted by the duty cycle of AGN activity; the duty cycle is the fraction of SMBHs that are "active" at any time. Thus, while easy to measure, the luminosity function provides somewhat limited physical insight. Fortunately, we have other empirical tools based on AGN demographics that provide various complementary observational constraints on SMBH growth and fueling. These include spatial clustering of AGNs, AGN host galaxy properties, and black hole mass and Eddington ratio distributions as a function of redshift. Spatial clustering provides observational constraints on the masses of AGN host dark matter halos, the bias of AGN environments, and AGN duty cycle. AGN host galaxy properties, on the other hand, provide insight into the fueling and triggering of AGN activity, as well as the effects of AGN feedback. And finally, studies of SMBH mass and Eddington ratio distributions provide insight into the growth of SMBHs and AGN duty cycles. These various empirical tools provide different but complementary information, and it is the goal of this work to further improve our understanding of SMBH mass and Eddington ratio distributions for Type 1 quasars.

The BHMF and black hole Eddington Ratio function (BHERF) quantify the comoving number density of SMBHs as a function of $M_{\rm BH}$ and $L/L_{\rm Edd}$. Therefore, the BHMF and BHERF provide a complete census of the SMBH population with respect to $M_{\rm BH}$ and $L/L_{\rm Edd}$, providing important information for constraining models of SMBH growth. Indeed, many models for SMBH growth have made predictions for the BHMF and BHERF at a variety of redshifts (e.g., Cattaneo et al. 2005; Di Matteo et al. 2008; Hopkins et al. 2008; Shen 2009; Tanaka & Haiman 2009; Volonteri & Begelman 2010; Fanidakis et al. 2011, 2012; Natarajan & Volonteri 2012; Draper & Ballantyne 2012). For a review of the BHMF of SMBHs, see Kelly & Merloni (2012).

There are two common approaches for estimating the BHMF and BHERF. The first approach is to employ a continuity equation describing the evolution of the SMBH population, and has its roots in the work of Soltan (1982). The basic idea behind these continuity equation methods is to assume a BHMF at very high redshift, use the AGN luminosity function as a probe of how fast the BHMF is changing, and then evolve the BHMF using the local BHMF as a constraint. The continuity equation methods also provide an estimate of the typical duty cycle and radiative efficiency of SMBHs, which can then be linked to a typical quasar lifetime and black hole spin, respectively. Several authors have derived the local BHMF for all SMBHs from individual sources using the scaling relationships between $M_{\rm BH}$ and host spheroidal properties (e.g., Salucci et al. 1999; Yu & Tremaine 2002; Aller & Richstone 2002; Marconi et al. 2004; Shankar et al. 2004, 2009b; Tundo et al. 2007; Yu & Lu 2008; Vika et al. 2009), providing the needed integral constraint for the continuity equation method. A number of groups have employed variations on the continuity equation technique (e.g., Yu & Tremaine 2002; Marconi et al. 2004; Merloni 2004; Hopkins et al. 2007b; Merloni & Heinz 2008; Shankar et al. 2009b; Cao 2010), and have generally concluded that most, if not all, of the local BHMF can be explained as the relic of AGN activity, with SMBH growth being dominated by periods when the SMBH was radiating near the Eddington limit. In addition, these studies have generally concluded that SMBH growth is anti-hierarchical, in agreement with the cosmic downsizing seen in the AGN luminosity function studies.

The other commonly employed approach to estimating the BHMF and BHERF is to use scaling relationships to obtain estimates of $M_{\rm BH}$ for individual sources, and then derive the BHMF and BHERF from the distribution of these estimates. Indeed, this approach provides the local BHMF needed for the continuity equation approach. It is also possible to incorporate scaling relationships into the continuity equation methods, as done by Merloni & Heinz (2008). The advantage of the scaling relationship approach is that the BHMF and BHERF at a given redshift is derived from the distribution of $M_{\rm BH}$ estimates, providing more information at that redshift than is provided by the local BHMF integral constraint used in the continuity equation methods. Unfortunately, the scaling relationship methods have the disadvantage that the host galaxy scaling relationships are currently only used to estimate the $z \approx 0$ BHMF and BHERF for all SMBHs. Many studies have found evidence for evolution in the SMBH-host galaxy scaling relationships (e.g., Treu et al. 2004, 2007; Peng et al. 2006; Woo et al. 2008; Decarli et al. 2010; Merloni et al. 2010; Bennert et al. 2010, but see Lauer et al. 2007; Shen & Kelly 2010; Schulze & Wisotzki 2011, and Portinari et al. 2012 for cautionary notes), and, while there have been attempts to estimate the BHMF based on an assumed form of the evolution in the scaling relationships (Tamura et al. 2006; Shankar et al. 2009a; Li et al. 2011), the quantitative form of the evolution has not been sufficiently precise to motivate widespread use of the scaling relationships to estimate BHMFs beyond the local universe.

For Type 1 quasars, an alternative to employing the host galaxy scaling relationships to estimate $M_{\rm BH}$ is to employ the so-called virial mass estimates (e.g., Wandel et al. 1999; McLure & Jarvis 2002; Vestergaard 2002; Vestergaard & Peterson 2006). These virial mass estimates are derived by using the width of the broad emission lines as a proxy for the velocity dispersion of the clouds emitting the broad emission lines, and the luminosity as a proxy for the broad-line region size (Kaspi et al. 2005; Bentz et al. 2009a; Greene et al. 2010a). The virial mass estimates have a statistical scatter about the mass estimates derived from reverberation mapping (Peterson et al. 2004; Bentz et al. 2009b)

of ∼0.4 dex (e.g., Vestergaard & Peterson 2006; Park et al. 2012b), although there may be additional systematic errors (Krolik 2001; Collin et al. 2006; Shen et al. 2008; Fine et al. 2008; Marconi et al. 2008; Denney et al. 2009; Rafiee & Hall 2011a; Steinhardt 2011). The virial and reverberation mapping mass estimates are calibrated to the local $M_{\rm BH}$–$\sigma^*$ relationship (Onken et al. 2004; Woo et al. 2010; Graham et al. 2011; Park et al. 2012a).

The virial mass estimates have the advantage that they can be used beyond the local universe, providing estimates of the BHMF and BHERF for active SMBHs directly from estimates of $M_{\rm BH}$. However, they have the disadvantage that they only estimate the BHMF for Type 1 quasars, which are a subset of the active SMBH population, which in turn is a subset of the entire SMBH population. However, despite this, the BHMF and BHERF for Type 1 quasars still provide an important observational constraint on models for SMBH growth that is complementary to other empirical tools based on AGN demographics. Compared to luminosity, studies of AGN demographics with respect to $M_{\rm BH}$ have the advantage that mass is a more stable quantity, in that $M_{\rm BH}$ can only increase and does so during active phases or through SMBH mergers. As a result, demographics of AGN $M_{\rm BH}$ probe the subset of SMBHs that are actively growing at any given $z$ and $M_{\rm BH}$. This implies that, for example, the Type 1 quasar BHMF provides an estimate of the SMBH duty cycle for Type 1 quasar activity as a function of $M_{\rm BH}$ and $z$, provided one has an estimate of the BHMF for all SMBHs at that redshift. Moreover, estimates of SMBH growth times for Type 1 quasars, calculated from the BHMF and BHERF, can also provide constraints on models for SMBH growth, especially at high redshift. In particular, the discovery of Type 1 quasars with $M_{\rm BH} \sim 10^9\,M_\odot$ out to $z \sim$ 6–7 (Jiang et al. 2007; Kurk et al. 2007; Willott et al. 2010; Mortlock et al. 2011) places strong constraints on models for the formation and growth of SMBH seeds (e.g., Haiman & Loeb 2001).

Numerous recent studies have used the virial mass estimates to study the demographics of Type 1 quasar $M_{\rm BH}$, Eddington ratio, and their evolution (e.g., Woo & Urry 2002; Vestergaard 2004; McLure & Dunlop 2004; Kollmeier et al. 2006; Sulentic et al. 2006; Babić et al. 2007; Netzer et al. 2007; Shen et al. 2008; Gavignaud et al. 2008; Fine et al. 2008; Trump et al. 2009, 2011; Trakhtenbrot et al. 2011; Rafiee & Hall 2011b). In particular, the use of virial mass estimates has led several authors to estimate the BHMF and BHERF for Type 1 quasars (Wang et al. 2006; Greene & Ho 2007; Vestergaard et al. 2008; Vestergaard & Osmer 2009; Kelly et al. 2009; Schulze & Wisotzki 2010; Kelly et al. 2010; Willott et al. 2010; Shen & Kelly 2010, 2012; Nobuta et al. 2012). In addition, $M_{\rm BH}$ is a fundamental physical parameter of black hole accretion flows, making the BHMF and BHERF important for studies of accretion physics, as it describes which regions of the $M_{\rm BH}$–$L/L_{\rm Edd}$ plane are probed by current and future surveys. Based on AGN number densities, several groups have found evidence for downsizing in $M_{\rm BH}$ of SMBHs in Type 1 quasars (e.g., Vestergaard & Osmer 2009; Labita et al. 2009a, 2009b; Kelly et al. 2010; Shen & Kelly 2012), implying that at least some of the downsizing in the AGN luminosity function may be driven by downsizing in $M_{\rm BH}$. In addition, the Eddington ratio distributions derived by Kelly et al. (2010, hereafter K10) and Shen & Kelly (2012) imply that at $z > 0.5$ there is a broad range in $L/L_{\rm Edd}$ for Type 1 quasars, and that most Type 1 quasars are not radiating near the Eddington limit; similar results were obtained by Schulze & Wisotzki (2010) at $z < 0.3$.

This is the second paper in a two-part series to study the demographics of Type 1 quasars out to $z \sim 4.75$ in the two-dimensional (2D) quasar mass and luminosity space. Such studies represent a next step in Type 1 quasar demographic studies by placing joint constraints on the distributions of their instantaneous activity (i.e., luminosity function) and assembly history (i.e., BH mass function) via the Eddington ratio distribution. As such, the 2D demographic studies provide an advanced view of the cosmic growth of the SMBH population compared with using the luminosity function or BHMF alone. Our study is motivated by both the recent availability of ∼58,000 uniformly selected Type 1 quasars from the Sloan Digital Sky Survey (SDSS) DR7 with virial mass estimates from Shen et al. (2011), as well as the recent advancements in statistical techniques for studying AGN demographics. The incredible size of this data set combined with our new powerful statistical tools provides us with an unprecedented ability to characterize the demographics of Type 1 quasars at a variety of redshifts. The broad redshift range of our sample ($0.4 < z < 4.75$) allows us to probe the evolution of a subset of the actively growing SMBH population during the epochs over which ∼95% of SMBH growth occurred (e.g., Shankar et al. 2009b).

### 1.2. Comparison with Shen & Kelly (2012)

In the first paper of this series, Shen & Kelly (2012, hereafter Paper I), we presented our sample as well as the binned estimates of the luminosity function and the BHMF. We also extended the statistical method of K10 to estimate the BHMF independently in different redshift bins, and to include a luminosity-dependent bias term for the virial mass estimates. The former improvement enables us to study the evolution of the BHMF and BHERF without assuming a parametric form for this evolution, while the latter improvement enables us to study the effects of a systematic error in the virial mass estimates with luminosity. A luminosity-dependent bias term is motivated by the small scatter in the virial mass estimates at fixed $M_{\rm BH}$ and $L$, as observed by several recent studies of AGN demographics (Kollmeier et al. 2006; Shen et al. 2008; Fine et al. 2008; Steinhardt & Elvis 2010b; Shen & Kelly 2010; K10). The results from our model implied that virial mass estimates derived from the FWHM of the Mg II and C IV emission lines systematically overestimate $M_{\rm BH}$ at higher than average luminosity, assuming that the statistical scatter in the mass estimates at fixed $M_{\rm BH}$ and $L$ is constant.

In Paper I we also used our model to study the luminosity function of Type 1 quasars, and presented the BHMF and BHERF derived from our model. We studied the luminosity function below the flux limit, assuming our model for the SMBH mass and Eddington ratio distributions. We found evidence for downsizing in both the luminosity function and BHMF. In addition, we found that our model luminosity function makes reasonable predictions when extrapolated to ∼3 mag fainter than our SDSS DR7 sample, and the extrapolations were often consistent with luminosity functions estimated from deeper surveys. We also found evidence that the average Eddington ratio of Type 1 quasars increases toward higher redshift, in qualitative agreement with the conclusions of continuity equation methods (e.g., Shankar et al. 2013) and predictions from recent hydrodynamic simulations of SMBH growth at $z > 4$ (e.g., DeGraf et al. 2012).

In this paper we build upon the work of Paper I and focus our analysis and discussion on the BHMF, the BHERF, and quantities that can be derived from them. The main differences between Paper I and this paper are as follows.

1. We make several improvements to our statistical model. We extend the statistical model of K10 and Paper I to model the joint distribution of Eddington ratio and $M_{\rm BH}$ at a given redshift as a mixture of 2D log-normal distributions. This provides us more flexibility compared with Paper I, where we assumed that the Eddington ratio distribution at fixed $z$ and $M_{\rm BH}$ could be described as a single log-normal distribution with geometric mean depending linearly on $\log M_{\rm BH}$. In addition, we also use a Student's $t$-distribution to model the distribution of measurement errors in the mass estimates, which downweights outliers compared to the previously used Gaussian distribution. This latter improvement was incorporated to make our results more robust against outliers in the mass–luminosity plane, as such sources may be subject to unidentified systematic error. We made these improvements to test the robustness of the key conclusions from Paper I.
2. Because we have employed a more flexible model for the BHERF, the focus of this paper is on the BHMF and BHERF of Type 1 quasars. As such, in this paper we discuss the BHMF and BHERF in greater depth than we did in Paper I, and discuss the distribution of Eddington ratios at fixed $M_{\rm BH}$. In addition, we discuss what the derived BHMF and BHERF imply with regard to the growth of SMBHs.
3. We focus our presentation and discussion on the BHMF and BHERF based on the usual assumption that the mass estimates are unbiased. This is the assumption that is typically made in the literature, but is different from Paper I where we allowed the mass estimates to have a luminosity-dependent bias. In this paper we present the results for the model assuming the estimates are unbiased, but also discuss how allowing a luminosity-dependent bias changes the results. Between Paper I and this paper we cover both simple models for the behavior of the virial mass estimates with respect to the BHMF and BHERF.
4. Unlike in Paper I, we do not present or discuss the optical luminosity function implied by our model, as there is little difference from Paper I, nor is the luminosity function the focus of this paper. Instead, we focus on the BHMF and BHERF.
5. Paper I goes into greater depth with respect to biases in the virial mass estimates, and what we can conclude about such biases based on AGN demographics. That is not the focus of this paper.

Between Paper I and this paper we present an in-depth analysis of Type 1 quasar demographics with respect to the properties of their virial mass estimates, their luminosity function, their BHMF, their BHERF, and their behavior in the mass–luminosity plane.

This paper is organized as follows. We describe our statistical model in Section 2. We present our estimated BHMF in Section 3 and BHERF in Section 4, and discuss our results in Section 5. We summarize our results in Section 6. Throughout the paper we adopt a flat ΛCDM cosmology with cosmological parameters $\Omega_\Lambda = 0.7$, $\Omega_0 = 0.3$, $h = 0.7$, to match most of the recent quasar demographics studies. Volume is in comoving units unless otherwise stated. We distinguish virial masses from true masses with a subscript $_{\rm vir}$. For simplicity, quasar luminosity is expressed in terms of the rest-frame 2500 Å continuum luminosity ($L \equiv \lambda L_\lambda$). The conversion between the 2500 Å continuum luminosity and the absolute $i$-band magnitude normalized at $z = 2$ ($M_i[z = 2]$) is given by Equation (4) in Richards et al. (2006). Lower case letters refer to logarithms of quantities based on mass or luminosity, e.g., $l \equiv \log L$, $m_{\rm BH} \equiv \log M_{\rm BH}$.

## 2. THE STATISTICAL MODEL AND POSTERIOR DISTRIBUTION

Early estimates of the BHMF were obtained by directly binning up the virial mass estimates and applying the $1/V_{\rm max}$ correction, where the $1/V_{\rm max}$ correction is the same as that used to estimate the luminosity function. However, BHMFs obtained in this manner suffer from both incompleteness caused by the sample flux limit and artificial broadening caused by the statistical error in the virial mass estimates (Kelly & Bechtold 2007; Shen et al. 2008; Kelly et al. 2009). The incompleteness arises because there is a large range in luminosity at fixed $M_{\rm BH}$, scattering some quasars at fixed $M_{\rm BH}$ above the flux limit and some below. The artificial broadening arises because the statistical error in the virial mass estimates scatters more quasars into bins of higher $M_{\rm BH}$ than lower $M_{\rm BH}$ when the BHMF declines toward higher values of $M_{\rm BH}$. In order to account for these effects, Kelly et al. (2009) developed a Bayesian technique for estimating both the BHMF and BHERF of Type 1 quasars that corrects for incompleteness and the effects of statistical error in the virial estimates; they used their method to estimate the local BHMF of Type 1 quasars. Schulze & Wisotzki (2010) developed and used a similar method to estimate the local BHMF and BHERF of Type 1 quasars, although they did not correct for the error in the virial mass estimates. Subsequent work presented in K10 and Paper 1 has improved upon the model of Kelly et al. (2009).

In this work we expand on the statistical model described in Paper 1. Kelly et al. (2009) modeled the distribution of Type 1 quasars in the mass–redshift plane as a mixture of log-normal distributions, and the Eddington ratio distribution at fixed $M_{\rm BH}$ as a single log-normal distribution whose geometric mean depended linearly on $\log M_{\rm BH}$. They assumed that the mass estimates were unbiased. Kelly et al. (2010) expanded this model and used a mixture of log-normals for the Eddington ratio distribution at fixed $M_{\rm BH}$. In both Kelly et al. (2009, 2010) the Eddington ratio distribution was assumed to not evolve, while in Paper 1 we incorporated evolution by estimating the BHMF and BHERF independently in different redshift bins. In this section we describe our expansion to the model of Paper I and summarize the important aspects of our statistical model; further details can be found in Paper I and Kelly et al. (2009).

### 2.1. Mixture of Log-normal Functions Model

Motivated by the observed small statistical scatter in the mass estimates for the SDSS, Paper I expanded on the model of Kelly et al. (2009) to incorporate a more flexible model for the error distribution of the mass estimates. In both Paper I and this paper the error distribution is modeled as a Gaussian distribution with unknown variance and optionally and unknown mean. Because we use FWHM-based virial mass estimates, our model is only with respect to these mass estimates; mass estimates based on the line dispersion or other line width measures may have a different error distribution. Paper I assumed that the mass estimates were unbiased at the average luminosity as a function of $M_{\rm BH}$, but that the mass estimates potentially exhibited a luminosity-dependent bias at fixed mass. They assumed the following model for the mass estimates:

$$m_{\rm vir} = m_{\rm BH} + \beta[l - E(l|m_{\rm BH})] + \sigma_{ml}\epsilon_{ml}. \quad (1)$$

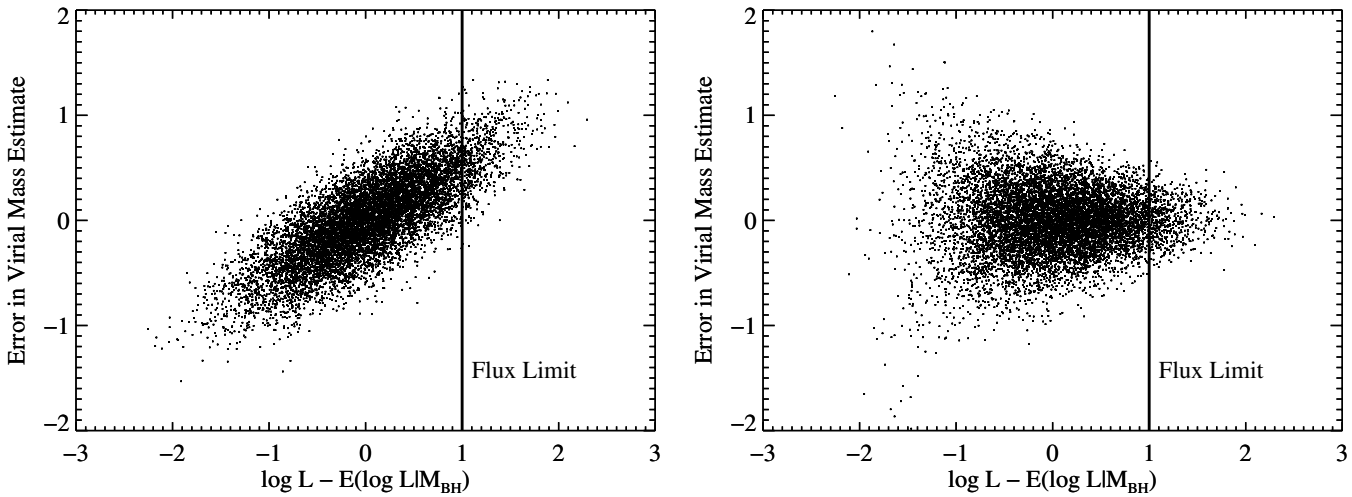


**Figure 1.** Illustration of the two models for the distribution of virial mass estimate errors used in this work. Mock data are generated using Equation (1). In both panels $E(\log L|M_{\rm BH})$ denotes the mean value of $\log L$ at fixed $M_{\rm BH}$. The left panel shows a model with a luminosity-dependent bias ($\beta > 0$) and constant $\sigma_{ml}$ with luminosity, while the right panel shows a model with $\beta = 0$ and a decrease in the amplitude of the error in the mass estimates toward higher $L$. In both models the dispersion in virial estimates decreases when limited to only those quasars in the bright tail of the luminosity distribution. However, the virial mass estimates are also biased if the small dispersion in mass estimates observed in the SDSS is caused by the situation depicted in the left panel ($\beta > 0$).

Here, $m_{\rm vir} \equiv \log M_{\rm vir}$, $m_{\rm BH} \equiv \log M_{\rm BH}$, $l \equiv \log L$, $E(l|m_{\rm BH})$ is the expectation value of $\log L$ at fixed $M_{\rm BH}$ and $\epsilon_{ml}$ is a random variable drawn from the standard normal distribution. The term $\beta$ models how the systematic error (i.e., the luminosity-dependent bias) in the mass estimates scales with luminosity, and $\sigma_{ml}$ is the standard deviation in the mass estimates at fixed $M_{\rm BH}$ and $L$. The standard mass estimates assume $\beta = 0$ and $\sigma_{ml} \sim 0.4$ dex.

The motivation for modeling the mass estimates according to Equation (1) is illustrated in Figure 1. Here we show the distribution of the error in the mass estimates at fixed true mass as a function of luminosity, assuming a value of $\beta = 0.5$ and $\sigma_{ml} = 0.25$. When averaging over a broad range of luminosity, as is done for the reverberation mapping sources, the distribution of the mass estimate errors is broad. However, when limiting ourselves to a narrow luminosity range at the bright end, as in a flux-limited sample like the SDSS, the mass estimates exhibit a bias and smaller scatter. This model is thus one way of reconciling the fact that the scatter in the mass estimates for the SDSS imply smaller uncertainties in $M_{\rm vir}$ than does the scatter in the mass estimates for the reverberation mapping sample. Some physical reasons to expect such a luminosity-dependent bias were further discussed in Section 3.2.1 of Paper I. Alternatively, another possibility is that the mass estimates at fixed mass and luminosity are always unbiased (i.e., $\beta = 0$), but $\sigma_{ml}$ decreases toward higher luminosity. This possibility is also illustrated in Figure 1. Currently it is not possible to unambiguously distinguish between these two possibilities solely from AGN demographics, and both situations may be at work. As discussed in Paper I, there is some indication from the reverberation mapping data for NGC 5548 that $\beta > 0$ for FWHM-based virial mass estimates, although this result is only moderately significant at $2.4\sigma$. As such, in this work we obtain constraints on the BHMF and Eddington ratio distribution under each of these two models for the error in the mass estimates.

The values of $\beta$ and $\sigma_{ml}$ are assumed to be different when different emission lines are used to calculate $M_{\rm vir}$. In this work we use the H$\beta$, Mg II, and C IV emission lines. These lines have different advantages and disadvantages, and the behavior of the mass estimates derived from the Mg II and C IV lines are less well understood than those derived from H$\beta$. We refer the reader to Paper I for a discussion of the issues and possible biases surrounding virial mass estimates derived from different emission lines (see also Shen & Liu 2012, and the discussion in Section 5.6).

In this work we model the joint distribution of $M_{\rm BH}$ and $L$ for Type 1 quasars in a given redshift bin as a mixture of $K$ 2D log-normal distributions:

$$p(m_{\rm BH}, l|\pi, \mu, \Sigma) = \times \sum_{k=1}^{K} \frac{\pi_k}{2\pi|\Sigma_k|^{1/2}} \exp\left\{-\frac{1}{2}(\mathbf{x}-\mu_k)^T\Sigma_k^{-1}(\mathbf{x}-\mu_k)\right\}. \quad (2)$$

Here, $\mathbf{x} = [m_{\rm BH}, l]^T$, $\mathbf{x}^T$ denotes the transpose of $\mathbf{x}$, $\pi = (\pi_1, \ldots, \pi_K)$, $\mu = (\mu_1, \ldots, \mu_K)$, and $\Sigma = (\Sigma_1, \ldots, \Sigma_K)$. The terms $\pi$ denote the relative contribution of each 2D Gaussian function to the model distribution, the terms $\mu$ denote the means of each Gaussian function in the $M_{\rm BH}$–$L$ plane, and the terms $\Sigma$ denote the covariance matrices of each Gaussian function in the $M_{\rm BH}$–$L$ plane. Note that Equation (2) is with respect to the true values of $M_{\rm BH}$, and not with the respect to the virial mass estimates; Equation (1) describes how to connect the distribution of the virial mass estimates to Equation (2).

As in Paper I we model the distribution of $z$ in each redshift bin as a Pareto distribution (i.e., a power law):

$$p(z|\gamma) = \frac{(1+\gamma)z^{\gamma}}{z_{\rm max}^{1+\gamma} - z_{\rm min}^{1+\gamma}}. \quad (3)$$

In this work we use a value of $K = 5$, which provides considerable flexibility. There was little difference in employing larger values of $K$ and such larger values did not justify the increased computational burden. Note that the comoving number density per three-dimensional box defined by $(m_{\rm BH}, l, z)$ and $(m_{\rm BH}, l, z) + (dm_{\rm BH}, dl, dz)$ is

$$\phi(m_{\rm BH}, l, z) = N\left(\frac{dV}{dz}\right)^{-1} p(m_{\rm BH}, l|\pi, \mu, \Sigma)p(z|\gamma), \quad (4)$$

where $N$ is the total number of Type 1 quasars in the observable universe, and $dV/dz$ is the derivative of comoving volume with

respect to redshift. The mass or luminosity function is obtained by integrating Equation (4) over $l$ or $m_{\rm BH}$, respectively.

In the absence of measurement error, Equations (1)–(3) provide us with all of the necessary ingredients to construct the likelihood function; i.e., these equations tell us how to connect the mass and luminosity functions to the observed distribution of virial mass estimates, luminosities, and redshifts. However, in reality the line widths and luminosities are measured with error, and therefore so are the virial mass estimates. In general, the measurement error on the FWHM dominates over the measurement error on the luminosity, so we only account for measurement errors on the virial mass estimates. Denote the measured virial mass estimate as $\hat{M}_{\rm vir}$ ($\hat{m}_{\rm vir} \equiv \log \hat{M}_{\rm vir}$). In this work we model the measurement error distribution of the virial mass estimates using a Student's $t$-distribution centered at the true value of $M_{\rm vir}$:

$$p(\hat{m}_{\rm vir}|m_{\rm vir}) = \times \frac{\Gamma((\nu+1)/2)}{\sigma_{\rm meas}\Gamma(\nu/2)\sqrt{\nu\pi}} \left[1 + \frac{1}{\nu}\left(\frac{\hat{m}_{\rm vir} - m_{\rm vir}}{\sigma_{\rm meas}}\right)^2\right]^{-(\nu+1)/2}. \quad (5)$$

Here, $\nu$ is the degrees of freedom of the $t$-distribution, $\sigma_{\rm meas}$ is the fixed measurement error amplitude, which is calculated from the emission line fitting procedure, and $\Gamma(\cdot)$ is the Gamma function. We use the Student's $t$-distribution because it is considered a robust alternative to the normal distribution. In the limit $\nu \to \infty$ the $t$-distribution converges to the normal distribution, but for finite $\nu$ the $t$-distribution has heavier tails. As a result, the $t$-distribution downweights the influence of outlying values of the virial mass estimates, which may be caused by systematics involving bad line width measurements, or due to the presence of a population of AGNs for which the virial mass estimates are subject to a large systematic error. In this work we use $\nu = 8$, which is a typical value for robust analysis; there is little difference in using similar values of $\nu$. This is a slight improvement over Paper I, where we modeled the measurement error distribution as a normal distribution.

For a given redshift bin, denote the set of parameters for our statistical model as $\theta = (\pi, \mu, \Sigma, \gamma, \beta, \sigma_{ml})$, the vector of measured virial masses as $\hat{\mathbf{M}}_{\rm vir}$, the vector of measured luminosities as $\mathbf{L}$, the vector of measured redshifts as $\mathbf{z}$, and the number of Type 1 quasars in our sample as $n$. Following Kelly et al. (2009), we derive the posterior distribution from Equations (1)–(3) and (5) as

$$p(\theta|\hat{\mathbf{M}}_{\rm vir}, \mathbf{L}, \mathbf{z}) = p(\theta)[p(I=1|\theta)]^{-n} \times \prod_{i=1}^{n} p(z_i|\gamma) \int_{-\infty}^{\infty} p(\hat{m}_{{\rm vir},i}|m_{{\rm vir},i}) p(m_{{\rm vir},i}, l_i|\theta) dm_{{\rm vir},i}, \quad (6)$$

where

$$p(m_{{\rm vir},i}, l_i|\theta) = \times \sum_{k=1}^{K} \frac{\pi_k}{2\pi|V_k|^{1/2}} \exp\left\{-\frac{1}{2}(\mathbf{x}_{{\rm vir},i} - \mu_k)^T V_k^{-1} (\mathbf{x}_{{\rm vir},i} - \mu_k)\right\} \quad (7)$$

$$\mathbf{x}_{{\rm vir},i} = [m_{{\rm vir},i}, l_i]^T \quad (8)$$

$$V_k = \begin{pmatrix} Var(m_{\rm vir}|k) & Cov(m_{\rm vir}, l|k) \\ Cov(m_{\rm vir}, l|k) & \Sigma_{L,k} \end{pmatrix} \quad (9)$$

$$Var(m_{\rm vir}|k) = \Sigma_{M,k} + \beta^2\left(\Sigma_{L,k} - \Sigma^2_{ML,k}/\Sigma_{M,k}\right) + \sigma^2_{ml} \quad (10)$$

$$Cov(m_{\rm vir}, l|k) = \Sigma_{ML,k} + \beta\left(\Sigma_{L,k} - \Sigma^2_{ML,k}/\Sigma_{M,k}\right). \quad (11)$$

Here, $p(\theta)$ is the prior on $\theta$, $n$ is the total number of data points in the redshift bin, $p(I = 1|\theta)$ is the probability of a Type 1 quasar from the redshift bin of interest making it into our sample, $V_k$ is the covariance matrix of $\log M_{\rm vir}$ and $\log L$ for the $k$th log-normal function, and $\Sigma_{M,k}$, $\Sigma_{L,k}$, and $\Sigma_{ML,k}$ denote the variance in $\log M_{\rm BH}$, variance in $\log L$, and covariance between $\log M_{\rm BH}$ and $\log L$ for the $k$th log-normal function, respectively. Equation (7) is obtained by averaging Equation (2) over the distribution of $m_{\rm vir}|m_{\rm BH}, l$ implied by Equation (1) with respect to $m_{\rm BH}$. The parameters, $\theta$, are estimated independently in each redshift bin.

As in Paper I, we define $L$ to be the luminosity at 2500 Å, which we derive from the $i$-band magnitude according to the prescription given in Richards et al. (2006). The term $p(I = 1|\theta)$ is the probability of including a Type 1 quasar in our sample given the model luminosity function, and is calculated from the SDSS selection function, $s(L, z)$, as

$$p(I=1|\theta) = \int_0^\infty \int_0^\infty s(L,z) p(L|\pi,\mu,\Sigma) p(z|\gamma)\, dL\, dz. \quad (12)$$

The selection function of our sample is the same as that for the sample in Richards et al. (2006), given in that paper.

### 2.2. The Prior Distribution

Flexible models such as the mixture of log-normal functions model that we use enable modeling of a broad range of distributions, but they can also suffer from overfitting because the data do not provide enough information on the structure of the distributions. It is often useful to impose priors invoking smoothness on the estimated distributions, otherwise highly "wiggly" BHMFs are considered just as likely as smooth ones a priori. In addition, because our sample is truncated, there is little to no information from the data on the distribution in the $M_{\rm BH}$–$L$ plane below the flux limit. Therefore, it is necessary to impose several constraints on $\theta$ via the prior distribution in order to keep the solution from wandering into unreasonable regions.

The prior constraints that we impose are as follows.

1. The standard deviation of each log-normal function must be between 0.2 and 1.0 dex for both $\log M_{\rm BH}$ and $\log L/L_{\rm Edd}$.
2. The mean of $\log M_{\rm BH}$ for each log-normal function must be between 6.0 and 10.0. This reflects our assumption that the BHMF must decrease at $M_{\rm BH} < 10^6\, M_\odot$ and $M_{\rm BH} > 10^{10}\, M_\odot$.
3. The mean value of $\log L/L_{\rm Edd}$ for each log-normal function must be between −3.0 and 0.0. The lower bound was chosen because accretion flows are thought to undergo a state transition near $L/L_{\rm Edd} \sim 10^{-2}$–$10^{-3}$, and the broad-line region is not expected to exist below this critical Eddington ratio (e.g., Czerny et al. 2004; Hopkins et al. 2009; Trump et al. 2011). The upper bound was chosen to reflect our assumption that the BHERF must decrease above the Eddington limit.

4. The fraction of Type 1 quasars in each log-normal function radiating at $\log L/L_{\rm Edd} < -3.5$ must be less than 1%. This constraint was added in addition to the constraint on the mean value of $\log L/L_{\rm Edd}$ to ensure that the estimated distribution of Type 1 quasars declined strongly at $L/L_{\rm Edd} \lesssim 10^{-3}$.

In order to test how sensitive our results are to these prior constraints, we have also performed the analysis allowing the standard deviation for both $\log M_{\rm BH}$ and $\log L/L_{\rm Edd}$ to be as high as 2.0 dex, and extending the lower limit for the mean value of $\log L/L_{\rm Edd}$. Extending the upper bound on $\Sigma_{M,k}$ does not significantly change our results beyond slightly increasing the uncertainties, with the only exception being that derived value for the maximum value of $M_{\rm BH}$ in the observable universe for a Type 1 quasar is very sensitive to this upper bound; this is discussed further in Section 3.3. In addition, the shape of the BHMF and BHERF at $M_{\rm BH} \gtrsim 3 \times 10^8\, M_\odot$ and $L/L_{\rm Edd} \gtrsim 0.05$ are not sensitive to the lower bound on the mean value of $\log L/L_{\rm Edd}$. However, the normalization of the BHMF and BHERF is sensitive to this lower bound, as this lower bound is directly related to how many Type 1 quasars our sample is missing. Luckily this is not a problem for our analysis as none of our scientific conclusions depend on the absolute normalization of the BHMF and BHERF.

Beyond the bounds listed above, we use a prior for the log-normal parameters that is based on the "partially proper prior" of Roeder & Wasserman (1997). We constrain the $K$ log-normal functions by ordering their values of $\mu_k$ by increasing mean luminosity, i.e., the $k = 1$ log-normal function has the faintest mean luminosity, and the $k = K$ log-normal function has the brightest. In addition, denote $\mu_{L,k}$ and $\mu_{M,k}$ to be the components of $\mu_k$ corresponding to the mean $\log L$ and $\log M_{\rm BH}$, respectively. Our prior for the luminosity components of $\theta$ is

$$p(\mu_L, \Sigma_L) = p(\mu_{L,1}) \prod_{k=2}^{K} p(\mu_{L,k}, \Sigma_{L,k} | \mu_{L,k-1}, \Sigma_{L,k-1}) \quad (13)$$

$$p(\mu_{L,1}) = \frac{\mu_{L,1} - l_{\rm min}}{l_{\rm min} - l_{\rm max}} \left(1 - \frac{\mu_{L,1} - l_{\rm min}}{l_{\rm min} - l_{\rm max}}\right)^{K-1} \quad (14)$$

$$p(\mu_{L,k}, \Sigma_{L,k} | \mu_{L,k-1}, \Sigma_{L,k-1}) = \times \frac{1}{2\pi h(k, k-1)} \left[\Phi\left(\frac{l_{\rm max} - \mu_{L,k-1}}{h_L(k, k-1)}\right) - \frac{1}{2}\right]^{-1} \times N(\mu_{L,k} | \mu_{L,k-1}, h_L(k, k-1)) H(\mu_{L,k} - \mu_{L,k-1}) \quad (15)$$

$$h_L(k, k-1) = 2\left(\frac{1}{\Sigma_{L,k}} + \frac{1}{\Sigma_{L,k-1}}\right)^{-1}. \quad (16)$$

Here, $l_{\rm min}$ and $l_{\rm max}$ are the minimum and maximum possible values of $\mu_{L,k}$, $h_L(k, k-1)$ denotes the harmonic mean of $\Sigma_{L,k}$ and $\Sigma_{L,k-1}$, $\Phi(\cdot)$ is the standard normal cumulative distribution function, $N(x|\mu, V)$ denotes a Gaussian function in $x$ with mean $\mu$ and variance $V$, and $H(\cdot)$ is the Heaviside step function. Given our prior constraints, $l_{\rm min}$ is the value of $\log L$ for $M_{\rm BH} = 10^6\, M_\odot$ and $L/L_{\rm Edd} = 10^{-3}$, and $l_{\rm max}$ is the value of $\log L$ for $M_{\rm BH} = 10^{10}\, M_\odot$ and $L/L_{\rm Edd} = 1$. We chose the prior on $\mu_{L,1}$ because it is the probability distribution for the minimum value of a sample of $K$ random variables uniformly distributed between $l_{\rm min}$ and $l_{\rm max}$. The prior on $\mu_{L,k}$ for $k > 1$ was chosen to enforce smoothness in the estimated luminosity function, as it places higher probability on solutions where the individual log-normal functions are close together with respect to their average standard deviations. Our prior on $\mu_L$ was therefore constructed to not favor a particular value for the centroid of the luminosity function, under the constraints listed above, but to favor smooth luminosity functions.

We also place a similar "smoothness" prior on $\mu_M$, but without enforcing a particular ordering of the log-normal functions:

$$p(\mu_M | \Sigma_M, \bar{m}) = \prod_{k=1}^{K} \frac{1}{\sqrt{2\pi h_M}} \exp\left\{-\frac{1}{2}\frac{(\mu_{M,k} - \bar{m})^2}{h_M}\right\} \quad (17)$$

$$h_M = K\left(\sum \frac{1}{\Sigma_{M,k}}\right)^{-1}. \quad (18)$$

The "hyper-parameter" $\bar{m}$ is the mean value of the $\{\mu_{M,k}\}$ and is an additional parameter. We assume a uniform prior on $\bar{m}$ over all possible values; note that even though we do not place explicit bounds on $\bar{m}$, such bounds are implied by the bounds placed on $\mu_{M,k}$. We place uniform priors on $\Sigma_{L,k}$ and $\Sigma_{M,k}$ under the constraints given above. We obtain the prior on $\Sigma_{ML,k}$ by placing a uniform prior on the angle that the slope of the mean value of $\log L/L_{\rm Edd}$ as a function of $M_{\rm BH}$ makes with the horizontal. For $\pi$, we assume a Dirichlet prior with parameter $\alpha = 0.1$. Finally, we use the same prior on $\beta$ and $\sigma_{ml}$ as that described in Section 3.2.1 of Paper I, which is constructed to give results consistent with the reverberation mapping sample.

## 3. THE BLACK HOLE MASS FUNCTION

We applied our Bayesian method to our sample derived from the SDSS DR7 data set for both the model with a luminosity-dependent bias ($\beta \neq 0$) and the model with decreasing scatter in the mass estimates at higher luminosity ($\beta = 0$). For the latter model ($\beta = 0$) we do not explicitly fit for a dependence of $\sigma_{ml}$ on $L$, but rather just assume a single value of $\sigma_{ml}$ over the luminosity range in each redshift bin. This should be an adequate approximation as the luminosity range of our data set in each redshift bin is narrow. Details of the sample are described in Paper I

Assuming the model with a luminosity-dependent bias, we estimate the slopes of the bias to be $\beta_{\rm H\beta} \approx 0.1 \pm 0.1$, $\beta_{\rm Mg\,II} \approx 0.39 \pm 0.13$, and $\beta_{\rm C\,IV} \approx 0.40 \pm 0.11$ for the H$\beta$, Mg II, and C IV emission lines, respectively. For the $\beta \neq 0$ model we estimate the scatter in the mass estimates at fixed luminosity and BH mass to be $\sigma_{\rm H\beta} \approx 0.24 \pm 0.03$, $\sigma_{\rm Mg\,II} \approx 0.25 \pm 0.02$, and $\sigma_{\rm C\,IV} \approx 0.21 \pm 0.01$ for the H$\beta$, Mg II, and C IV emission lines, respectively. These values are significantly different from the traditionally assumed values of $\beta = 0$ and $\sigma_{BL} = 0.4$ dex. However, we note that at $z \gtrsim 3.5$ the derived values for the C IV line become $\beta_{\rm C\,IV} \approx 0.3 \pm 0.3$ and $\sigma_{\rm C\,IV} \approx 0.39 \pm 0.04$, probably reflecting the broader range in luminosity at these redshifts due to the deeper SDSS flux limit. This increase in $\sigma_{ml}$ as the range in luminosity is increased supports our hypothesis that the dispersion in the virial mass estimate error is luminosity dependent.

These results on the luminosity-dependent bias model are similar to that obtained in Paper I using a simpler model for the Eddington ratio distribution, showing that many of the results of Paper I are robust against the assumed Eddington

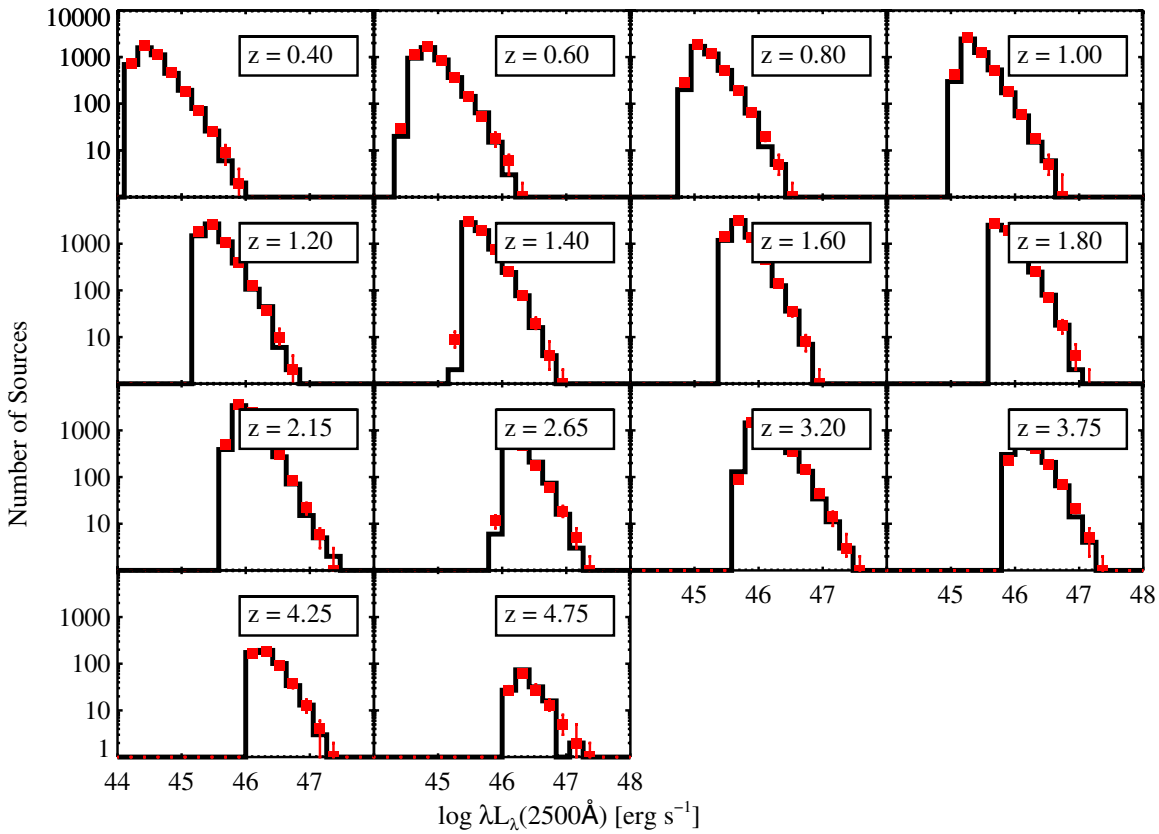


**Figure 2.** Posterior predictive check comparing the actual distribution of luminosities for our sample (solid histogram) with the set of distributions generated by our black hole mass and Eddington ratio functions (red squares with error bars). The error bars contain 68% of the posterior probability. The distributions of luminosities generated by our model are consistent with the observed distributions, showing that our model provides an acceptable fit.

(A color version of this figure is available in the online journal.)

ratio distribution. We therefore conclude from this that either the statistical scatter in the FWHM-based broad-line mass estimates is correlated with luminosity, producing a luminosity-dependent bias, or that the scatter in the mass estimates is smaller for the luminous quasars probed by the SDSS, or some combination of these two possibilities. In Paper I we have already discussed the implications of these results for the broad-line mass estimates, and, as the focus of this paper is on the Type 1 quasar BHMF and Eddington ratio distribution, we merely note here that our earlier conclusions on the statistical properties of the broad-line mass estimate errors are unchanged using a more flexible model for the Eddington ratio distribution.

For the sake of brevity, in the remainder of this work we present the results obtained from the model that assumes that there is no luminosity-dependent bias, i.e., $\beta = 0$. We do this for easier comparison with other work, as almost all studies implicitly assume that there are no systematic trends in the mass estimate errors with luminosity. However, we also discuss what aspects of our results change when we allow the mean value of the error in the mass estimates to depend on luminosity.

### 3.1. Evaluating the Fit Quality

In order to evaluate whether our model provides a good fit to the data, we use a technique called posterior predictive check (Rubin 1981, 1984; Gelman et al. 1996). For each random draw of the BHMF, the BHERF, and the values of $\sigma_{ml}$ from their joint posterior probability distribution we generate a mock sample of virial mass estimates and luminosities, conditional on the SDSS quasar selection function. These mock samples are then compared to the actual data to check for consistency. This approach therefore includes our uncertainty in the BHMF and BHERF, as well as the randomness in generating a single sample from the BHMF and BHERF.

In Figures 2 and 3 we compare the histograms of the luminosities and virial mass estimates for our sample with the histograms of the mock samples generated from our MCMC output. Our estimated BHMF and BHERF generate samples of the virial mass estimates and luminosities that are consistent with our actual data, showing that our model provides an acceptable fit. The mock samples generated by the model that includes a luminosity-dependent bias term were also consistent with the data.

### 3.2. Comoving Number Densities as a Function of $M_{BH}$ and $z$

Our estimated BHMF and its uncertainty in various redshift bins is shown in Figure 4 and reported in Table 1. The best-fit BHMF is defined as the posterior median value of the number density as a function of $M_{\rm BH}$, and the uncertainty in the BHMF is defined to be the region containing 68% of the posterior probability for the number density as a function of $M_{\rm BH}$. Note that this represents the formal statistical uncertainty on the BHMF; in reality, the actual uncertainty is larger due to unaccounted for systematic errors. Also shown in Figure 4 is the estimated 10% completeness limit and the flux-limited BHMF for quasars at $i < 19.1$ at $z < 2.9$ and $i < 20.2$ at $z > 2.9$, corresponding to the approximate flux limits of the SDSS DR7 quasar sample.

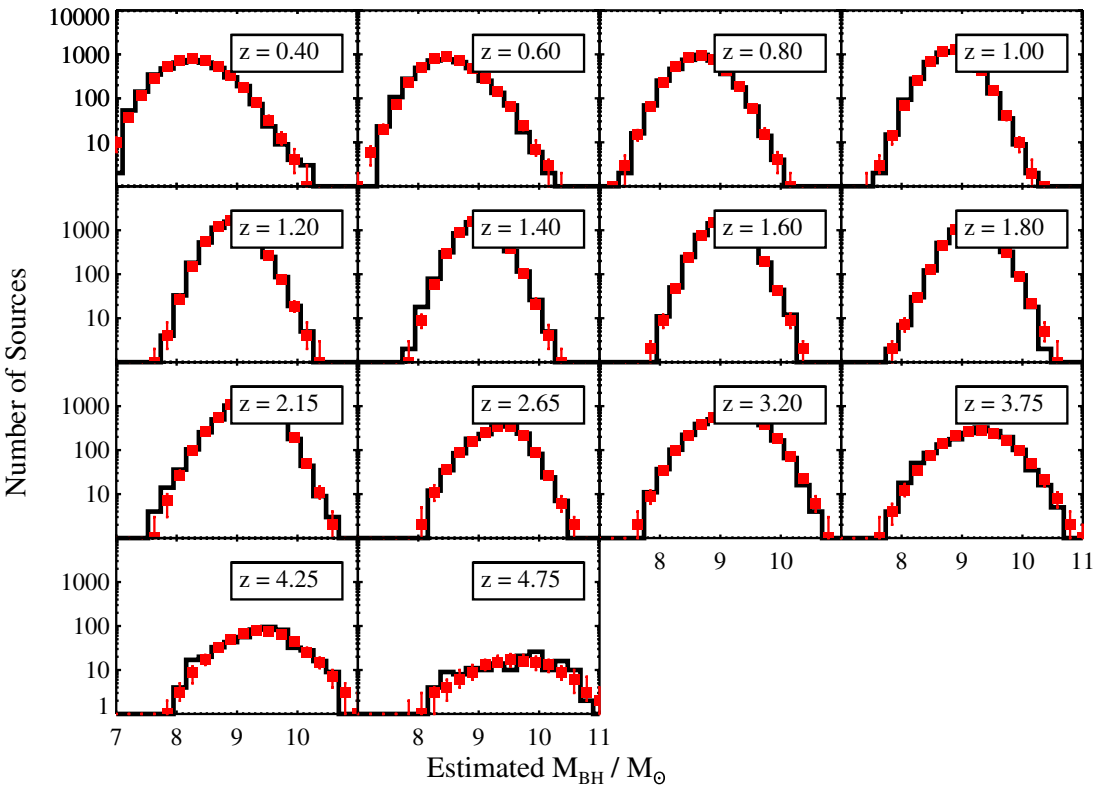


**Figure 3.** Same as Figure 2, but for the virial mass estimates from Shen et al. (2011). The distributions of virial masses generated by our model are consistent with the observed distributions, showing that our model provides an acceptable fit.

(A color version of this figure is available in the online journal.)

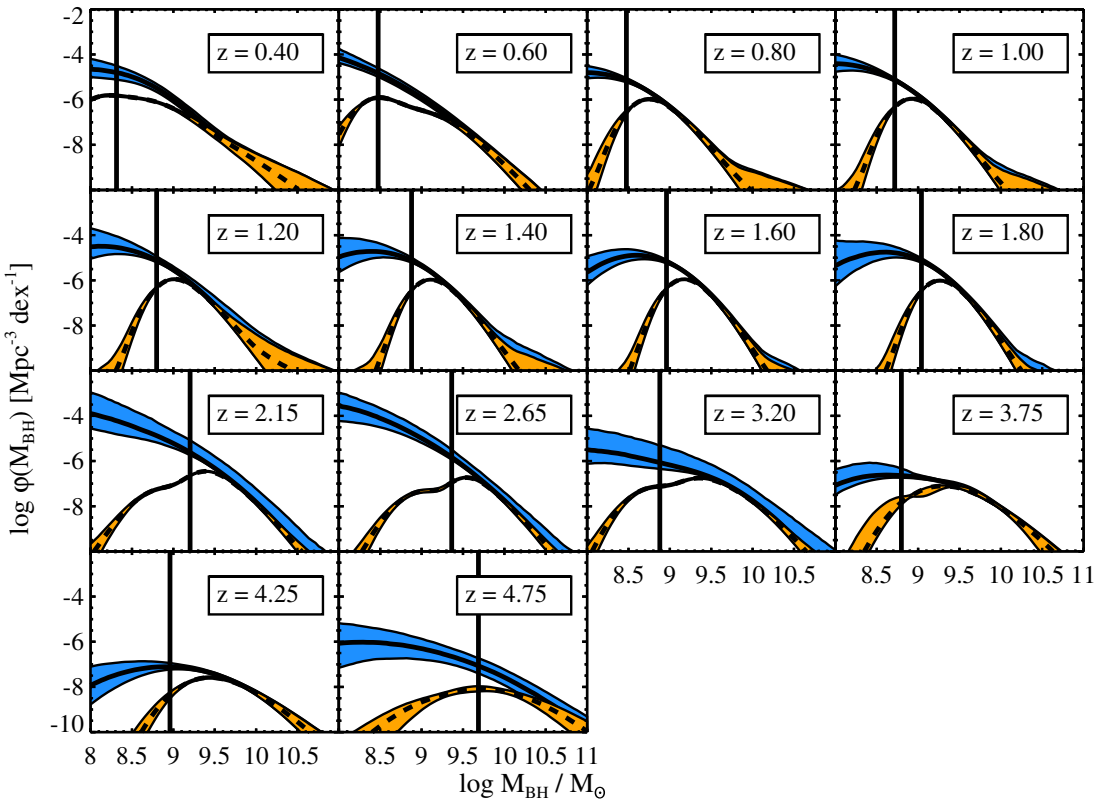


**Figure 4.** Black hole mass function for broad-line AGNs derived from our sample. The blue region contains 68% of the probability for the BHMF, and the solid line running through it denotes the best-fit BHMF, defined to be the posterior median. The orange shaded region contains 68% of the probability on the BHMF for Type 1 quasars above the SDSS flux limits, and the dashed line denotes the posterior median. The vertical solid line denotes the mass below which the completeness in the BHMF drops to $\lesssim$10% for the flux-limited SDSS sample, and thus mass bins below this marker are highly incomplete and the extrapolation becomes highly uncertain. We do not find any evidence for a turnover in the Type 1 quasar BHMF above the 10% completeness limit in $M_{BH}$.

(A color version of this figure is available in the online journal.)

**Table 1**
Type 1 Quasar Black Hole Mass Functions

| $\bar{z}$ | $\log M_{\rm BH}$ ($M_\odot$) | $\log \Phi_-$ [a] | $\log \Phi_0$ [b] ($\rm Mpc^{-3}\ dex^{-1}$) | $\log \Phi_+$ [c] |
|---|---|---|---|---|
| 0.400 | 8.000 | −5.00 | −4.64 | −4.21 |
| 0.400 | 8.100 | −5.03 | −4.67 | −4.30 |
| 0.400 | 8.200 | −5.06 | −4.72 | −4.39 |
| 0.400 | 8.300 | −5.09 | −4.78 | −4.50 |
| 0.400 | 8.400 | −5.14 | −4.87 | −4.62 |
| 0.400 | 8.500 | −5.22 | −4.97 | −4.76 |
| 0.400 | 8.600 | −5.32 | −5.12 | −4.92 |
| 0.400 | 8.700 | −5.47 | −5.29 | −5.09 |
| 0.400 | 8.800 | −5.65 | −5.49 | −5.31 |
| 0.400 | 8.900 | −5.87 | −5.72 | −5.54 |
| 0.400 | 9.000 | −6.12 | −5.97 | −5.80 |
| 0.400 | 9.100 | −6.40 | −6.25 | −6.08 |
| 0.400 | 9.200 | −6.70 | −6.54 | −6.37 |
| 0.400 | 9.300 | −7.02 | −6.84 | −6.67 |
| 0.400 | 9.400 | −7.32 | −7.14 | −6.96 |
| 0.400 | 9.500 | −7.61 | −7.43 | −7.25 |
| 0.400 | 9.600 | −7.89 | −7.70 | −7.52 |
| 0.400 | 9.700 | −8.17 | −7.96 | −7.76 |
| 0.400 | 9.800 | −8.48 | −8.19 | −7.97 |
| 0.400 | 9.900 | −8.79 | −8.41 | −8.16 |
| 0.400 | 10.00 | −9.10 | −8.63 | −8.33 |
| 0.400 | 10.10 | −9.44 | −8.85 | −8.51 |
| 0.400 | 10.20 | −9.79 | −9.09 | −8.66 |
| 0.400 | 10.30 | −10.1 | −9.33 | −8.82 |
| 0.400 | 10.40 | −10.4 | −9.57 | −8.97 |
| 0.400 | 10.50 | −10.8 | −9.83 | −9.12 |
| 0.400 | 10.60 | −11.2 | −10.1 | −9.28 |
| 0.400 | 10.70 | −11.5 | −10.3 | −9.43 |
| 0.400 | 10.80 | −11.9 | −10.6 | −9.58 |
| 0.400 | 10.90 | −12.3 | −10.9 | −9.76 |
| 0.400 | 11.00 | −12.7 | −11.2 | −9.94 |

**Notes.** Tabulated here are the results for the $\beta = 0$ error model. Results for the $\beta \neq 0$ error model are similar to those presented in Paper I.
[a] Lower boundary on the region containing 68% of the posterior probability for the BHMF, i.e., the 16th percentile of the posterior distribution.
[b] Posterior median for the BHMF.
[c] Upper boundary on the region containing 68% of the posterior probability for the BHMF, i.e., the 84th percentile of the posterior distribution.
(This table is available in its entirety in a machine-readable form in the online journal. A portion is shown here for guidance regarding its form and content.)

It is apparent that our sample starts to become significantly incomplete at $M_{\rm BH} \lesssim 3 \times 10^8\ M_\odot$, and any conclusions from the BHMF at these masses become reliant on our model for the BHMF and our assumptions for deriving it from the mass estimates. In addition, extrapolation in our BHMF is unstable against small unidentified errors in both the SDSS selection function and the mass estimates beyond the region where we are reasonably complete. As discussed in K10, to zeroth order the BHMF can be estimated as $\phi_M(M_{\rm BH}) \sim n(M_{\rm BH})/s(M_{\rm BH})$, where $n(M_{\rm BH})$ is the measured number density of Type 1 quasars with mass $M_{\rm BH}$, and $s(M_{\rm BH})$ is the Type 1 quasar completeness as a function of $M_{\rm BH}$. The term $s(M_{\rm BH})$ is calculated by averaging the SDSS selection function over the luminosity distribution at fixed $M_{\rm BH}$ (see Equation (11) in Kelly et al. 2009). The estimated BHMF is highly sensitive to both the measured number of sources in a mass bin and the value of $s(M_{\rm BH})$ when $s(M_{\rm BH})$ is very small, and thus is unstable against even small errors in $n(M_{\rm BH})$ and the selection function.

The Type 1 quasars in the most incomplete bins tend to be those with the lowest signal-to-noise (S/N) spectra. Because the FWHM measurement can be biased in low S/N spectra (Denney et al. 2009), the measured number densities of the most incomplete mass bins may be incorrect due to biases in the mass estimates derived from FWHM measurements, which would scatter objects into incorrect mass bins. In addition, the SDSS quasar selection function is derived via simulation by Richards et al. (2006). Aspects of this simulation that are not representative of the quasar population (e.g., lack of a host galaxy component) can introduce errors into the quasar selection function, which are manifested as errors in $s(M_{\rm BH})$. Therefore, in order to limit the impact of systematics, we focus our discussion on the regions of parameter space where the SDSS DR7 is $\gtrsim$10% complete.

In general, the BHMF falls off approximately as a power law toward higher mass $M_{\rm BH}$, with the BHMF being steeper at higher mass. The comoving number density of SMBHs in Type 1 quasars continues to increase all the way down to the masses corresponding to the ≈10% completeness limits, and thus we do not observe a peak in the BHMF from the SDSS. Instead, we constrain the peak in the Type 1 quasar BHMF to occur at $M_{\rm BH} \lesssim 2 \times 10^8\ M_\odot$.

In Figure 5 we show the evolution in the Type 1 quasar BHMF at four different values of $M_{\rm BH}$. The number densities of SMBHs in Type 1 quasars with $M_{\rm BH} \lesssim 10^9\ M_\odot$ fall off more steeply toward higher redshift at $z \gtrsim 2$, while the number densities of $M_{\rm BH} \gtrsim 10^9\ M_\odot$ fall off more steeply with decreasing redshift at $z \lesssim 2$. These trends imply that more massive black holes are more likely to be observed at higher $z$ in Type 1 quasars than less massive ones. These trends have been called "downsizing," and have been observed in previous work (e.g., Vestergaard & Osmer 2009; K10; Paper I). In addition, there is evidence for a discontinuity in the number densities across the redshift where we switch from H$\beta$ to Mg II when calculating the mass estimates. This discontinuity may be partly driven by systematic differences in the H$\beta$- and Mg II-based mass estimates. However, it is also likely driven at least in part by the contribution from a host galaxy component to the nuclear emission which boosts the number of Type 1 quasars above the flux limit at $z \lesssim 0.8$, but is not modeled in the selection function (Richards et al. 2006). Considering this, it is likely that the number densities at $z \lesssim 0.8$ are overestimated, especially at $z = 0.4$.

In Figure 6 we compare the mass functions derived from both models for the error distribution in the virial mass estimates at three representative redshifts. There is little difference in the BHMFs derived from our models with and without a luminosity-dependent bias in the mass estimates, with the exception that the BHMF derived from Mg II and C IV is shifted toward lower values of $M_{\rm BH}$ by $\approx$ 0.2 dex for the model that includes a luminosity-dependent bias (i.e., $\beta \neq 0$). In addition the uncertainties in the BHMF are larger when we allow for a luminosity-dependent bias. We also note that the BHMF for the $\beta \neq 0$ error model is consistent with that presented in Paper I, but with larger uncertainties on account of the more flexible Eddington ratio distribution model.

While the derived BHMF does not depend strongly on the existence of a luminosity-dependent bias, the flux-limited BHMF does depend strongly on the value of $\beta$. This is because the segment of the SMBH population that is probed within a certain luminosity range depends strongly on how the errors in the mass estimates scale with luminosity. However, this is not a concern, as the flux-limited BHMF is not of interest in this work. However, it would be a concern, for instance, when

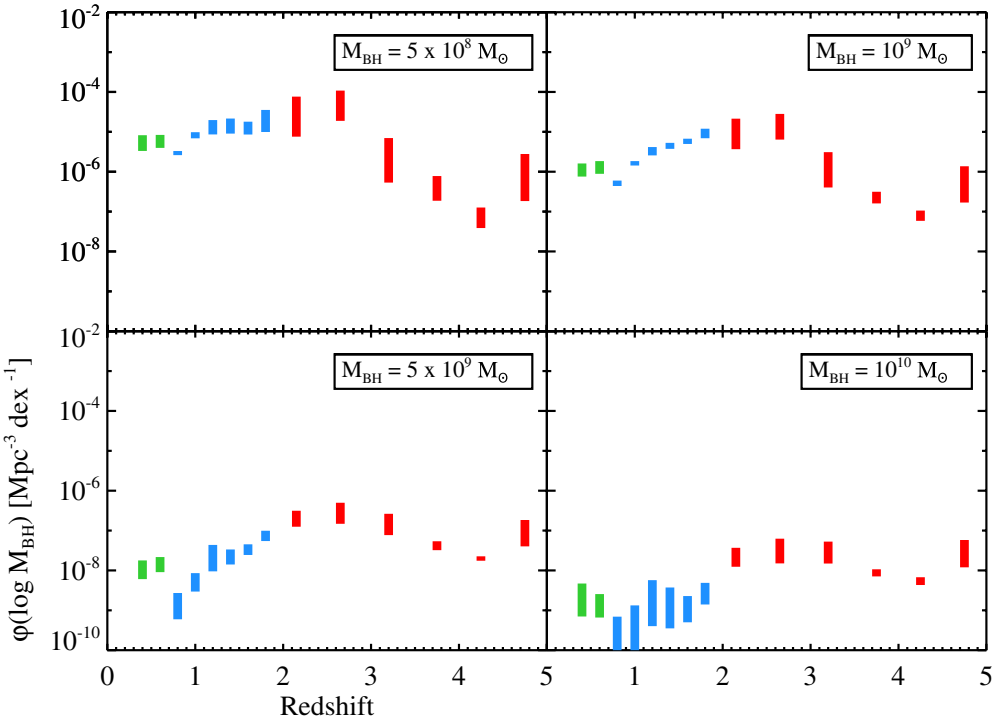


**Figure 5.** Evolution in the comoving number densities of Type 1 quasars at four different values of $M_{\rm BH}$. The bars contain 68% of the posterior probability. The green bars denote bins with H$\beta$-based virial mass estimates, the blue bars denote bins with Mg II-based mass estimates, and the red bars denote bins with C IV-based mass estimates. All of the bins show a peak in the number density around $z \sim 2$, with the higher mass bins falling off more steeply toward lower redshift and less steeply toward higher redshift, relative to the peak. The trend is commonly referred to as "downsizing."

(A color version of this figure is available in the online journal.)

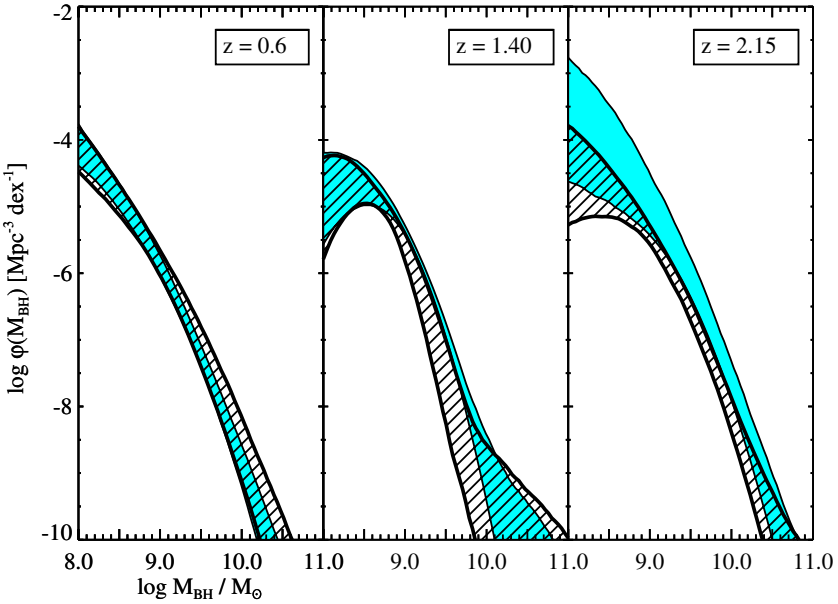


**Figure 6.** Comparison of the BHMF derived from the model with a luminosity-dependent bias ($\beta \neq 0$, diagonal line-filled region) and without a luminosity-dependent bias ($\beta = 0$, cyan region). For simplicity, we only show one redshift for each emission line used to calculate the virial mass estimates; the omitted bins exhibit similar differences. There is no apparent difference in the BHMFs derived from the H$\beta$ line, while the BHMFs derived from the Mg II and C IV lines under the model with $\beta \neq 0$ are shifted lower in $M_{\rm BH}$ by $\approx$0.2 dex. This is a rather small difference and in general our scientific conclusions do not change when we allow a luminosity-dependent bias.

(A color version of this figure is available in the online journal.)

using virial black hole mass estimates from flux-limited samples to investigate models for accretion flows or evolution of the BH–bulge scaling relation at high redshift (e.g., Shen & Kelly 2010).

### 3.3. How Massive can Black Holes Become?

Following K10, we compute the probability distribution of $M_{\rm BH}^{\rm max}(z)$, the most massive SMBH from a population of

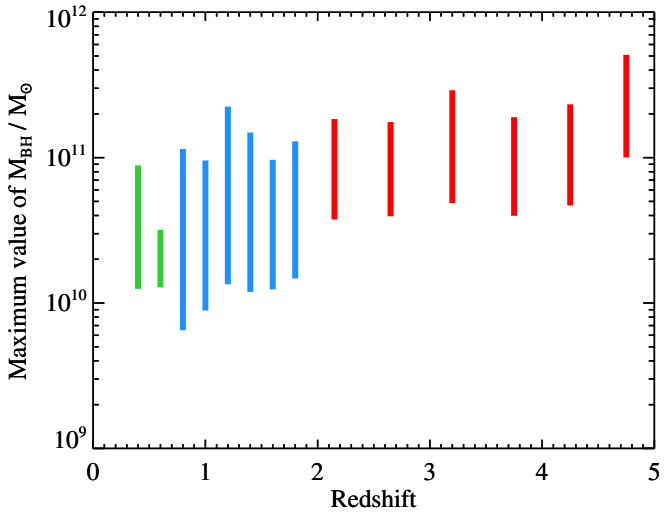


**Figure 7.** Constraints on the maximum mass that could be observed in a broad-line quasar as a function of redshift. Symbols are as in Figure 5. The maximum value of $M_{\rm BH}$ for quasars implied by our BHMF is $M_{\rm BH}^{\rm max} \sim 4 \times 10^{10}\,M_\odot$, although values of $10^{10} < M_{\rm BH}^{\rm max}/M_\odot < 10^{11}$ are consistent within the uncertainties. However, as discussed in the text the values of $M_{\rm BH}^{\rm max}$ we derive are highly sensitive to our adopted prior constraints, and the values shown should be treated as lower limits.

(A color version of this figure is available in the online journal.)

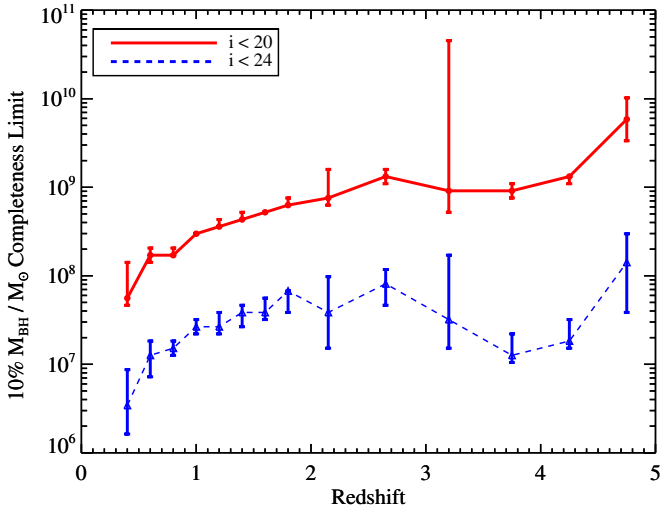


**Figure 8.** Values of $M_{\rm BH}$ at which a Type 1 quasar survey becomes only 10% complete under a limiting magnitude of $i < 20$ (red solid line) and $i < 24$ (blue dashed line), as a function of redshift. The data points denote the posterior median values, and the error bars contain 68% of the posterior probability. The SDSS becomes highly incomplete below $M_{\rm BH} \sim 3 \times 10^8\,M_\odot$.

(A color version of this figure is available in the online journal.)

Type 1 quasars drawn from the BHMF within each redshift bin. In other words, this quantity may be thought of as the most massive SMBH that would have been observed within each redshift bin in an all-sky survey of Type 1 quasars without a flux limit. The probability distribution for the maximum value of $M_{\rm BH}$ generated by a random draw from the BHMF is calculated as

$$p\big(\log M_{\rm BH}^{\rm max}|\pi,\mu,\Sigma,N\big) = Np\big(\log M_{\rm BH}^{\rm max}|\pi,\mu,\Sigma\big) \times \left[\int_{-\infty}^{\log M_{\rm BH}^{\rm max}} p(m_{\rm BH}|\pi,\mu,\Sigma)\,dm_{\rm BH}\right]^{N-1}, \quad (19)$$

where $p(m_{\rm BH}|\pi,\mu,\Sigma)$ is obtained by marginalizing Equation (2) over luminosity. In order to incorporate our uncertainty on the derived BHMF, we calculate Equation (19) for each value of $(N,\pi,\mu,\Sigma)$ returned by our MCMC sampler and average the results.

Our derived constraints on $M_{\rm BH}^{\rm max}(z)$ are shown in Figure 7. There are no obvious trends between $M_{\rm BH}^{\rm max}(z)$ and redshift, although there may be a slight trend for $M_{\rm BH}^{\rm max}(z)$ to be larger at higher $z$. This is consistent with "downsizing," but may also be due to larger systematic errors in C IV-based mass estimates. The results for the luminosity-dependent bias model are very similar, but the uncertainties are ~30% larger.

As mentioned in Section 2.2 our derived constrained on $M_{\rm BH}^{\rm max}$ are sensitive to the prior placed on $\Sigma_{M,k}$. This is because large value of $\Sigma_{M,k}$ imply tails in the BHMF that extend to larger value of $M_{\rm BH}$, and therefore larger values of $M_{\rm BH}^{\rm max}$. If we constrain $\Sigma_{M,k} < 2$ instead of $\Sigma_{M,k} < 1$, then the upper boundary of the error bars on $M_{\rm BH}^{\rm max}$ extends to $M_{\rm BH} \sim 10^{12}$–$10^{13}\,M_\odot$. Ideally the prior should not have a strong influence on this quantity, but unfortunately the upper flux limit for the SDSS results in the extreme high mass tail of the BHMF being poorly constrained; because of the upper flux limit, there is nothing in the data from prohibiting a small population of Type 1 quasars hosting SMBHs with, say, $M_{\rm BH} \sim 10^{12}\,M_\odot$. Considering this, we can formally only place a lower bound of $M_{\rm BH}^{\rm max} \sim 10^{10}\,M_\odot$ on the maximum mass in the observable universe of a SMBH in a Type 1. This is consistent with the range $2 \times 10^{10}\,M_\odot \lesssim M_{\rm BH}^{\rm max} \lesssim 5 \times 10^{10}\,M_\odot$ at $z > 1$ that K10 estimated from their sample based on the SDSS DR3.

### 3.4. Completeness in Black Hole Mass

In Figure 8 we show the 10% completeness limit in $M_{\rm BH}$ as a function of $z$ for a Type 1 quasar survey with a flux limit of $i < 20$ and $i < 24$. In calculating these completeness limits we assume a step function down to the flux limit, i.e., we do not assume the SDSS selection function. The $i < 20$ flux limit roughly corresponds to the SDSS flux limit, while the $i < 24$ flux limit is similar to the limiting magnitude for the *Pan-STARRS* Medium Deep Survey Fields (Saglia et al. 2012) as well as the spectroscopic samples from *COSMOS* (e.g., Lilly et al. 2007; Trump et al. 2007). As with other quantities derived in this section, the results from the model with a luminosity-dependent bias in the mass estimates are similar but with larger uncertainties. Samples with a limiting magnitude of $i = 20$ start to become strongly incomplete at $M_{\rm BH} \sim 10^8\,M_\odot$ by $z \sim 1$, increasing to $M_{\rm BH} \sim 7 \times 10^8\,M_\odot$ by $z \sim 2$. However, Type 1 quasar samples with a limiting magnitude of $i = 24$ are able to go an order of magnitude "deeper" in $M_{\rm BH}$, becoming incomplete at $M_{\rm BH} \sim 10^7\,M_\odot$ by $z \sim 1$ and $M_{\rm BH} \sim 7 \times 10^7\,M_\odot$ by $z \sim 2$.

The contribution from the host galaxy is neglected in these calculations, but would likely become important near $i \sim 24$, at least at lower redshift. The host-galaxy contribution would affect these calculations in two ways. First, the host galaxy leads to an increase in nuclear emission, possibly moving the nuclear flux above the limiting magnitude, allowing one to detect intrinsically fainter Type 1 quasars. And second, the host galaxy dilutes the AGN emission, making it harder to identify whether the galaxy nucleus hosts a Type 1 quasar. The exact details of these effects will depend on the distribution of Type 1 quasar host galaxy luminosities and morphologies at fixed $M_{\rm BH}$, as well as the Type 1 quasar identification algorithm of a particular survey. As such, it is unclear how the host galaxy would affect the $M_{\rm BH}$

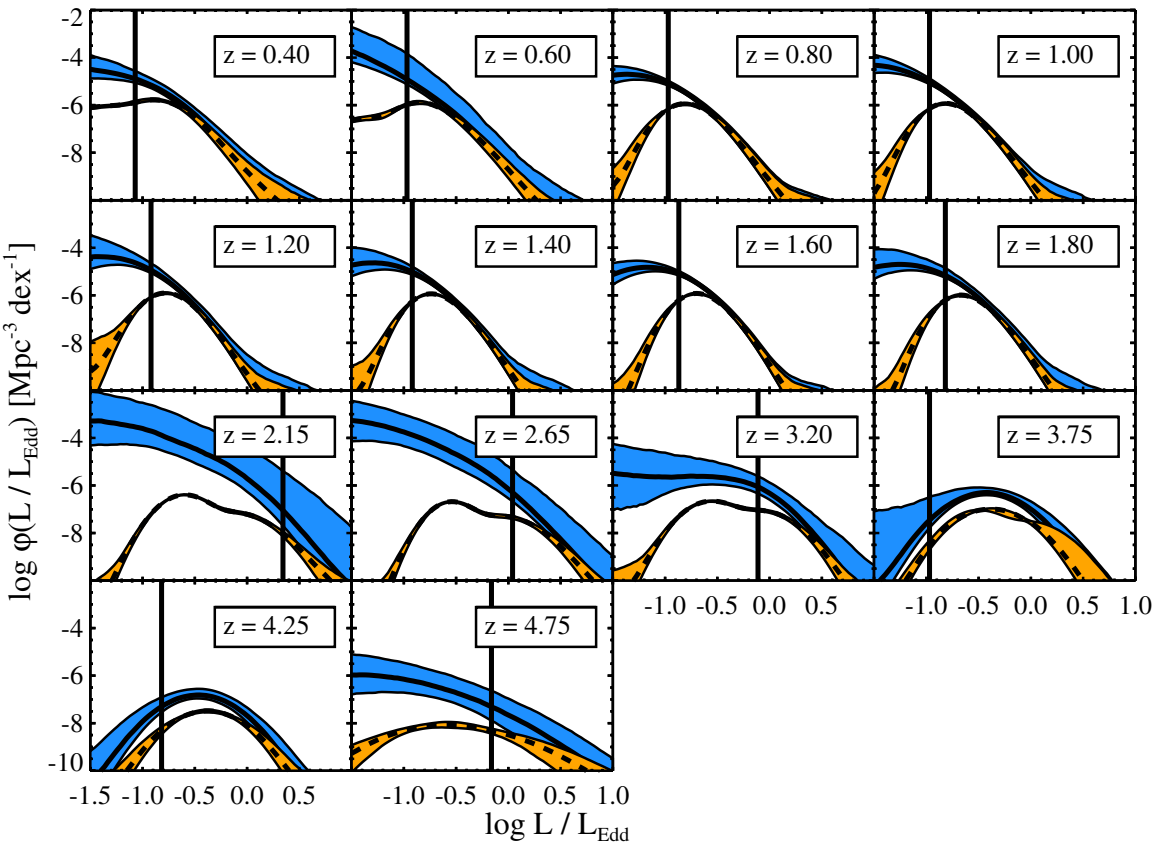


**Figure 9.** Black hole Eddington ratio function for broad-line AGNs derived from our sample. The labeling is the same as in Figure 9. There is a broad range in $L/L_{\rm Edd}$ for Type 1 quasars, and there is no evidence for a turnover in the BHERF down to $L/L_{\rm Edd} \sim 0.07$, except for possibly in the redshift range $3.20 \lesssim z \lesssim 4.75$.
(A color version of this figure is available in the online journal.)

completeness limits, and our estimated limits for $i < 24$ should merely be viewed as suggestive.

## 4. THE EDDINGTON RATIO DISTRIBUTION

### 4.1. Number Densities

Our estimated Type 1 quasar BHERF is shown in Figure 9 and reported in Table 2. Also shown is the flux-limited BHERF and the value of $L/L_{\rm Edd}$ below which our sample becomes <10% complete. As in Paper I, the BHERF was calculated from the model BHMF and luminosity function assuming a bolometric correction to $\nu L_\nu(2500\ \text{Å})$ of $C_{2500} = 5$. In general, the SDSS quasar sample is incomplete at $L/L_{\rm Edd} \lesssim 0.07$. The comoving number densities of SMBHs in Type 1 quasars increase toward lower Eddington ratio, a trend that continues beyond the incompleteness limit. The only exceptions are the $z = 3.75$ and $z = 4.25$ bins, which display evidence for a peak in the BHERF at $L/L_{\rm Edd} \approx 0.3$. However, the BHERFs in these bins are derived from the C IV line and may be subject to systematics resulting from an outflowing wind component (e.g., Shen et al. 2008; Richards et al. 2011), so it is unclear whether this peak is real. Indeed, the redshift bins before and after these two do not show any evidence for a peak in the BHERF, although they also employ the C IV line. In addition, we note that because we adopted a more flexible model for the Eddington ratio distribution, our constraint on the redshift evolution of the *mean* Eddington ratio is much poorer than that in Paper I, but is generally consistent with the trend found in Paper I.

Figure 10 shows the evolution in the comoving number densities at four different values of $L/L_{\rm Edd}$. The number densities at $L/L_{\rm Edd} \gtrsim 0.05$ are roughly constant at $z < 2$, implying that there is no "downsizing" in Eddington ratio at these redshifts. However, the number densities of Type 1 quasars radiating at $L/L_{\rm Edd} \lesssim 0.1$ decline rapidly at $z \gtrsim 3$ while the number densities of Type 1 quasars radiating at $L/L_{\rm Edd} \gtrsim 0.5$ are similar at $z \lesssim 2$ and $z \gtrsim 3$. This may be evidence for downsizing in Eddington ratio, in which the number densities of Type 1 quasars at low Eddington ratios increases rapidly from $z \sim$ 4–5 to $z \sim 3$. However, we caution that this trend is primarily driven by the $z = 3.75$ and $z = 4.25$ redshift bins, which are the only ones that show a peak in the BHERF above the SDSS completeness limit.

There is an apparent discontinuity in the number densities across $z \sim 2$, with the number densities at $z \sim 2.15$ being ~1–2 orders of magnitude larger than that at $z \sim 1.8$. While the uncertainties on the number densities at $2 < z < 3$ are large, making this only a $1\sigma$–$2\sigma$ effect, there are a couple of other issues with this redshift range that are worth commenting on. For one, $z \sim 2$ marks the transition between mass estimates calculated from Mg II and C IV, so there may be systematic differences among these lines. However, we do not see the same effect in the evolution of the BHMF, and the number densities of the virial mass estimates (i.e., the binned BHMF) typically show continuity between the redshift bins where the mass estimates switch emission lines (Paper I), suggesting that the use of different emission lines is not the dominant reason for this discontinuity. Instead, the apparent discontinuity in number density may be primarily due to systematic errors in

**Table 2**
Type 1 Quasar Black Hole Eddington Ratio Functions

| $\bar{z}$ | $\log L/L_{\rm Edd}$ | $\log \Phi_-$ [a] | $\log \Phi_0$ [b] ($\rm Mpc^{-3}\ dex^{-1}$) | $\log \Phi_+$ [c] |
|---|---|---|---|---|
| 0.400 | −1.50 | −4.83 | −4.45 | −3.89 |
| 0.400 | −1.40 | −4.84 | −4.52 | −4.00 |
| 0.400 | −1.30 | −4.86 | −4.60 | −4.15 |
| 0.400 | −1.20 | −4.91 | −4.69 | −4.31 |
| 0.400 | −1.10 | −5.00 | −4.83 | −4.48 |
| 0.400 | −1.00 | −5.13 | −4.98 | −4.68 |
| 0.400 | −0.90 | −5.31 | −5.18 | −4.91 |
| 0.400 | −0.80 | −5.54 | −5.41 | −5.17 |
| 0.400 | −0.70 | −5.83 | −5.70 | −5.45 |
| 0.400 | −0.60 | −6.17 | −6.02 | −5.76 |
| 0.400 | −0.50 | −6.57 | −6.40 | −6.11 |
| 0.400 | −0.40 | −7.03 | −6.81 | −6.49 |
| 0.400 | −0.30 | −7.54 | −7.25 | −6.90 |
| 0.400 | −0.20 | −8.09 | −7.72 | −7.31 |
| 0.400 | −0.10 | −8.65 | −8.18 | −7.70 |
| 0.400 | 0.000 | −9.22 | −8.63 | −8.08 |
| 0.400 | 0.100 | −9.79 | −9.08 | −8.46 |
| 0.400 | 0.200 | −10.3 | −9.49 | −8.77 |
| 0.400 | 0.300 | −10.8 | −9.88 | −9.07 |
| 0.400 | 0.400 | −11.3 | −10.2 | −9.37 |
| 0.400 | 0.500 | −11.9 | −10.6 | −9.61 |
| 0.400 | 0.600 | −12.5 | −10.9 | −9.85 |
| 0.400 | 0.700 | −13.1 | −11.3 | −10.0 |
| 0.400 | 0.800 | −13.6 | −11.6 | −10.3 |
| 0.400 | 0.900 | −14.1 | −12.0 | −10.5 |
| 0.400 | 1.000 | −14.6 | −12.3 | −10.7 |

**Notes.** Tabulated here are the results for the $\beta = 0$ error model. Results for the $\beta \neq 0$ error model are similar to those presented in Paper I.
[a] Lower boundary on the region containing 68% of the posterior probability for the BHERF, i.e., the 16th percentile of the posterior distribution.
[b] Posterior median for the BHERF.
[c] Upper boundary on the region containing 68% of the posterior probability for the BHERF, i.e., the 84th percentile of the posterior distribution.
(This table is available in its entirety in a machine-readable form in the online journal. A portion is shown here for guidance regarding its form and content.)

our incompleteness correction. The three redshift bins $z = 2.15, 2.65$, and 3.20 correspond to redshifts where quasars colors are similar to star colors, making the SDSS quasar color selection incomplete at these redshifts. The completeness can be as low as ∼5% in this redshift range. The color distribution of simulated quasars does not perfectly match the observed color distribution at these redshift (Richards et al. 2006), suggesting that there may be systematic uncertainties in the estimated selection function. In addition, the completeness of the selection algorithm at these redshifts depends on the quasar optical/UV spectral energy distribution (SED), which in turn has been found to depend on $L/L_{\rm Edd}$ (e.g., Bonning et al. 2007). However, any dependence of this completeness on $L/L_{\rm Edd}$ is not accounted for in the SDSS selection function, introducing systematic error if the quasar colors do depend on $L/L_{\rm Edd}$. Similarly, the Type 1 quasar bolometric correction also depends on $L/L_{\rm Edd}$ and $M_{\rm BH}$ (e.g., Vasudevan & Fabian 2007, 2009; Kelly et al. 2008). Our use of a constant bolometric correction may exasperate the systematics over this redshift range. Because the estimated number densities are unstable in bins of $L/L_{\rm Edd}$ that are significantly incomplete (see Section 3.2), there is likely a significant additional systematic uncertainty that is not reflected in the error bars on the number densities at $2 \lesssim z \lesssim 3.2$. Therefore, we do not consider the apparent discontinuity in the number densities at $z \sim 2.15$ to be real.

Unlike with the BHMF, the BHERF is noticeably different when we allow for a luminosity-dependent bias. In Figure 11 we compare the BHERF derived from the models with and without a luminosity-dependent bias for three representative redshift bins. This difference is negligible for the H$\beta$-based mass estimates, for which $\beta \approx 0$. However, in the redshift bins where Mg II and C IV mass estimates are used the model that includes the luminosity-dependent bias leads to BHERFs that are more uncertain and fall off flatter toward higher $L/L_{\rm Edd}$, implying a larger number of Type 1 quasars radiating near the Eddington limit. In addition, while the number densities at the high $L/L_{\rm Edd}$ end of the BHERF depend on the value of $\beta$, the evolution in the number densities at fixed $L/L_{\rm Edd}$ is not as affected by the value of $\beta$. The evolution results obtained for the luminosity-dependent bias model are not significantly different from those obtained for the $\beta = 0$ model.

### *4.2. Distribution of Eddington Ratio as a Function of Black Hole Mass*

In Figure 12 we show the conditional probability distribution of $\log L/L_{\rm Edd}$ at $M_{\rm BH} = 5 \times 10^8\ M_\odot$ and $M_{\rm BH} = 5 \times 10^9\ M_\odot$ for $z = (0.6, 1.6, 2.65)$; note that these quantities integrate to one and are not the same as the BHMF and BHERF. We show $p(\log L/L_{\rm Edd}|M_{\rm BH})$ for both the model which assumes $\beta = 0$ and the model with free $\beta$. As with the BHERF, the estimated conditional Eddington ratio distributions are broader and more uncertain, especially for the redshifts where the Mg II line is used.

In general the conditional Eddington ratio distributions mimic the behavior seen in Figure 12, with $p(\log L/L_{\rm Edd}|M_{\rm BH})$ being similar for $M_{\rm BH} = 5 \times 10^8\ M_\odot$ and $M_{\rm BH} = 5 \times 10^9\ M_\odot$ at $z \sim 0.6$, but with the distribution of $L/L_{\rm Edd}$ being shifted to larger values for $M_{\rm BH} = 5 \times 10^9\ M_\odot$ compared with $M_{\rm BH} = 5 \times 10^8\ M_\odot$. In addition, at higher redshifts the distributions of $\log L/L_{\rm Edd}|M_{\rm BH}$ exhibit a peak around $L/L_{\rm Edd} \sim 0.1$. The peak in $p(\log L/L_{\rm Edd}|M_{\rm BH})$ is below the SDSS completeness limit for $M_{\rm BH} \sim 5 \times 10^8\ M_\odot$ at $z \gtrsim 1.5$, so it is unclear if this is a real feature. On the other hand, for $M_{\rm BH} \sim 5 \times 10^9\ M_\odot$ this peak does occur above the completeness limit.

At both high ($z \gtrsim 3.2$) and low ($z \lesssim 0.6$) redshifts the $L/L_{\rm Edd}$ distribution is relatively independent of $M_{\rm BH}$. However, at redshifts $0.8 \lesssim z \lesssim 2.65$ the distribution of $L/L_{\rm Edd}$ at fixed $M_{\rm BH}$ shifts to larger Eddington ratios from $M_{\rm BH} \sim 5 \times 10^8\ M_\odot$ to $M_{\rm BH} \sim 5 \times 10^9\ M_\odot$. This therefore implies that at $0.8 \lesssim z \lesssim 2.65$ Type 1 quasars with more massive black holes are more likely to be radiating near the Eddington limit. However, we note that this redshift range is dominated by mass estimates derived from Mg II, and it is possible that systematic effects with this line may be driving some of these results. The results in the last two redshift bins in this range are derived from the C IV line mass estimates, and although they do show a shift in the distribution toward larger $L/L_{\rm Edd}$, for larger $M_{\rm BH}$ the difference in the Eddington ratio distributions at $M_{\rm BH} = 5 \times 10^8\ M_\odot$ and $M_{\rm BH} = 5 \times 10^9\ M_\odot$ are not as strong as that seen in the Mg II bins. In fact, in the two $z < 3$ bins that use the C IV estimate ($z = 2.15$ and $z = 2.65$), the fraction of Type 1 quasars radiating near the Eddington limit is the same for both mass bins within the uncertainties. The results from this section are similar for the model that includes a luminosity-dependent bias, with the exceptions that the distributions of $L/L_{\rm Edd}|M_{\rm BH}$ were broader and more uncertain.

These results are in contrast to the conclusions reached by Steinhardt & Elvis (2010a). These authors used virial mass

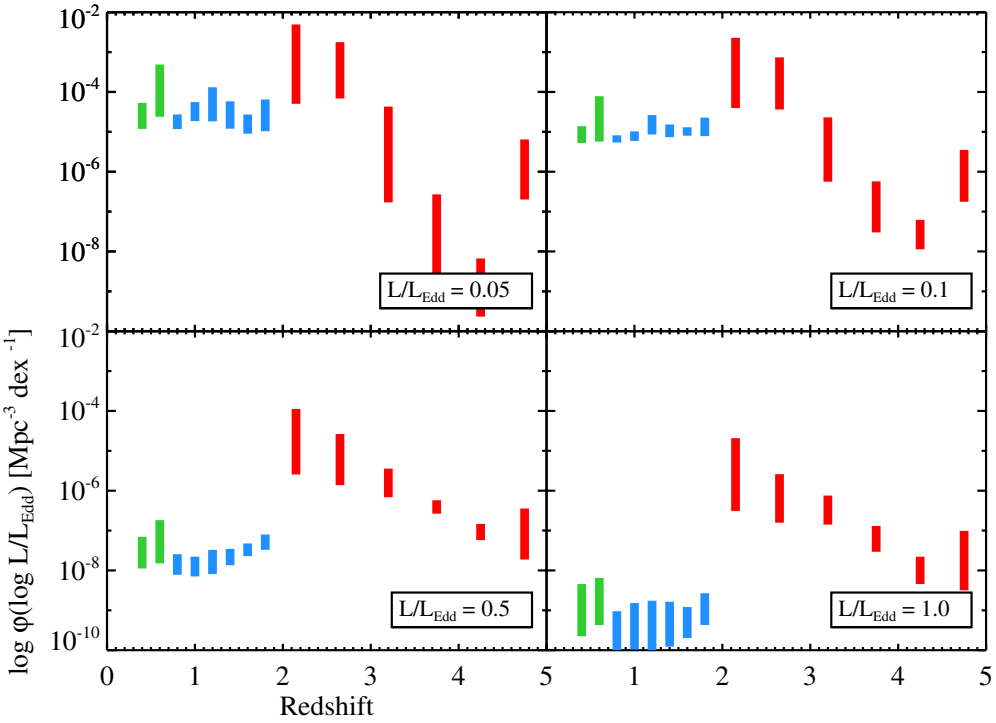


**Figure 10.** Evolution in the comoving number densities of Type 1 quasars at four different values of $L/L_{\rm Edd}$. The labeling is the same as in Figure 5. The number densities of Type 1 quasars are fairly constant in redshift below $z < 2$ for all Eddington ratio bins. However, the number densities of Type 1 quasars radiating at lower values of $L/L_{\rm Edd}$ drop off more steeply toward higher redshift at $z > 2$.

(A color version of this figure is available in the online journal.)

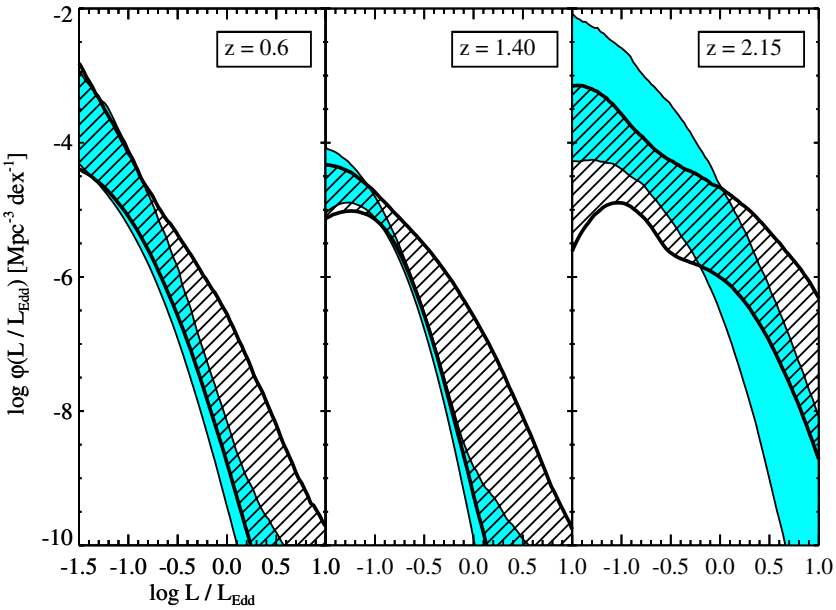


**Figure 11.** Same as Figure 6, but for the Eddington ratio function. Unlike for the BHMF, there is a more significant difference in the BHERFs derived under the two models for the virial mass estimate errors. In all cases the uncertainties on the BHERF are larger for the mode that includes a luminosity-dependent bias. In addition, the BHERF under the model with $\beta \neq 0$ is shifted toward higher values $L/L_{\rm Edd}$. This shift is small in the redshift bins using H$\beta$, but increases to $\approx 0.5$ dex for the redshift bins using Mg II and C IV.

(A color version of this figure is available in the online journal.)

estimates from the SDSS DR5 quasar sample of Shen et al. (2008) to argue that the most massive Type 1 quasars fall short of the Eddington limit, forming what they called a "sub-Eddington boundary" (but see Rafiee & Hall 2011a). Steinhardt & Elvis (2010a) quantified this trend through the 95th percentile of luminosities above the peak in the distribution of estimated bolometric luminosities for the sample, finding that the 95th percentile in luminosity increased slower with $M_{\rm BH}$ than would be expected from a constant value of $L/L_{\rm Edd}$. We consider the likely reason for their different conclusion to be uncorrected incompleteness. While it is true that for a flux-limited sample the 95th percentile in $L/L_{\rm Edd}$ at fixed $M_{\rm BH}$ mass does increase

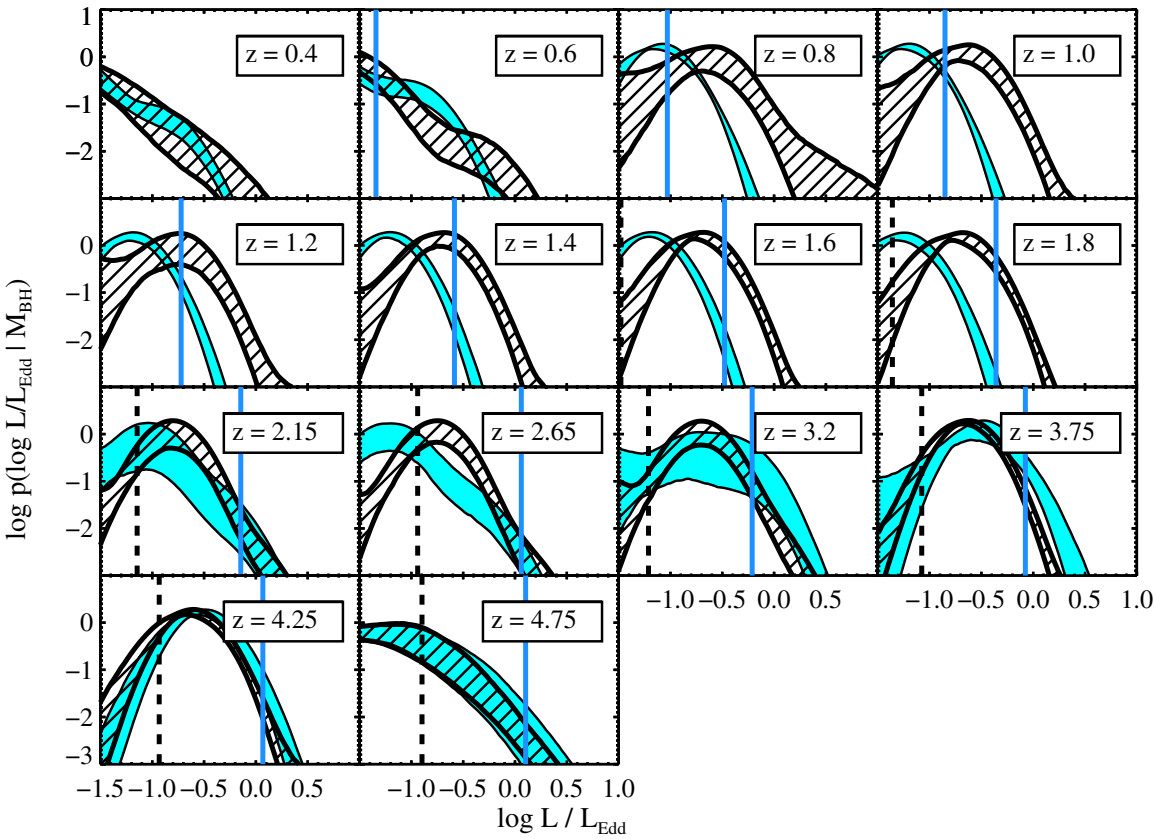


**Figure 12.** Conditional probability distributions for Eddington ratio at $M_{\rm BH} = 5 \times 10^8\ M_\odot$ (cyan region) and $M_{\rm BH} = 5 \times 10^9\ M_\odot$ (diagonal black line-filled region); both regions contain 68% of the posterior probability in $p(\log L/L_{\rm Edd}|M_{\rm BH})$ as a function of $M_{\rm BH}$. The solid blue vertical line marks the incompleteness limit in $L/L_{\rm Edd}$ for $M_{\rm BH} = 5 \times 10^8\ M_\odot$, while the vertical dashed black line marks the limit for $M_{\rm BH} = 5 \times 10^9\ M_\odot$. Note that for $M_{\rm BH} = 5 \times 10^9\ M_\odot$ the limit occurs below $\log L/L_{\rm Edd} = -1.5$ at $z \lesssim 1.6$.

(A color version of this figure is available in the online journal.)

with decreasing $M_{\rm BH}$, this is not necessarily true of the Type 1 quasar population as a whole. The reason for this is because the 95th percentile in $L/L_{\rm Edd}$ at fixed $M_{\rm BH}$ for a flux-limited sample is an overestimate of the true 95th percentile due to the loss of the faint end of the population. For smaller values of $M_{\rm BH}$ one loses a larger fraction of the lower $L/L_{\rm Edd}$ part of the population, increasing the bias in the 95th percentile inferred from the distribution of Type 1 quasars that are actually bright enough to be detected. Indeed, for the least massive black holes in a flux-limited sample one cannot even detect the 95th percentile of the Eddington ratio distribution, as it falls below the flux limit. This leads to a spurious increase in the 95th percentile of the $L/L_{\rm Edd}$ distribution with decreasing $M_{\rm BH}$. In addition, the errors of virial BH mass estimates stretch the distribution in the mass–luminosity plane along the mass direction, causing artificial flattening and an apparent "tilt" away from the Eddington limit toward higher virial BH masses (see Figure 8 of Paper I), which could be incorrectly recognized as visual evidence for a sub-Eddington boundary. However, we note that this effect is not as strong as the bias caused by incompleteness.

In this work we have corrected for incompleteness in flux-limited samples and errors in virial BH mass estimates, assuming our statistical model and the SDSS selection function, and thus attempt to recover the true intrinsic trends in the high $L/L_{\rm Edd}$ tail with $M_{\rm BH}$. Upon doing so, we do not find any evidence that higher mass Type 1 quasars are less likely to be observed at high $L/L_{\rm Edd}$, but in fact at certain redshifts may be more likely to have high $L/L_{\rm Edd}$. Therefore, the observed dearth of Type 1 quasars having both high $M_{\rm BH}$ and high $L/L_{\rm Edd}$ is not caused by a change in the shape of the tail of the Eddington ratio distribution, but is instead caused by the rapidly decreasing number densities of Type 1 quasars toward higher masses. Because the most massive SMBHs in Type 1 quasars are rare by definition, we would not expect those that we do observe to also occupy the rare high-$L/L_{\rm Edd}$ region of the mass–luminosity plane.

At low redshift past the peak of quasar activity, the most massive SMBHs are probably accreting mostly at very low Eddington ratios, but are no longer shining in the form of Type 1 quasars. We do not find any statistical evidence of a sub-Eddington boundary in the mass–luminosity plane of Type 1 quasars, and earlier claims of such a boundary are likely the result of uncorrected incompleteness.

### *4.3. Do quasars obey the Eddington Limit?*

Similar to the calculation of the maximum mass performed in Section 3.3, we can also calculate the probability distribution of the highest value of $L/L_{\rm Edd}$ from a population of Type 1 quasars drawn from our estimated BHERF. The maximum value of $L/L_{\rm Edd}$ as a function of redshift is shown in Figure 13. Our BHERF implies that the maximum value of $L/L_{\rm Edd}$ for a Type 1 quasar is $L/L_{\rm Edd} \sim 3$, although values between $L/L_{\rm Edd} = 1$ and $L/L_{\rm Edd} = 10$ are well within the uncertainties. The results from using the model with a luminosity-dependent bias suggest values of the maximum Eddington ratio a factor of $\sim$2 higher,

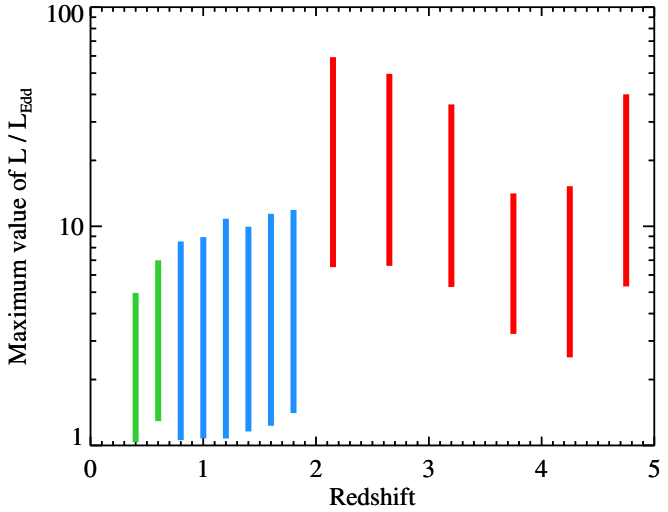


**Figure 13.** Constraints on the maximum Eddington ratio that could be observed in a broad-line quasar as a function of redshift. Symbols are as in Figure 5. There is no evidence for significantly super Eddington radiation, and the maximum value of $L/L_{\rm Edd}$ for quasars implied by our BHERF is $L/L_{\rm Edd} \sim 3$.

(A color version of this figure is available in the online journal.)

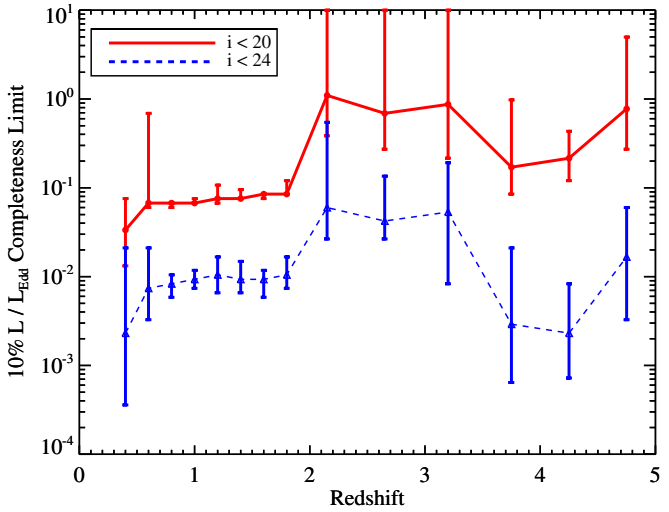


**Figure 14.** Values of $L/L_{\rm Edd}$ at which a Type 1 quasar survey becomes only 10% complete under a limiting magnitude of $i < 20$ and $i < 24$. The labeling is the same as in Figure 8. The SDSS becomes highly incomplete below $L/L_{\rm Edd} \sim 0.07$.

(A color version of this figure is available in the online journal.)

which is smaller than the uncertainties within individual redshift bins. The maximum values of $L/L_{\rm Edd}$ are somewhat divergent at $2 < z < 3.2$, having values near $L/L_{\rm Edd} \sim 10$, but, as discussed above, this range is subject to large statistical and systematic uncertainties. In addition, our results suggest that quasars at $z \sim 4$ may obtain a maximum value of $L/L_{\rm Edd}$ that is slightly larger than quasars at $z \lesssim 2$, but the error bars are large. Considering this, our results are consistent with a maximum value of $L/L_{\rm Edd} \sim 3$ across all redshift bins. In addition, there is additional systematic uncertainty in the maximum value of $L/L_{\rm Edd}$ caused by our assumption of a constant bolometric correction. Taking this into account, we do not find any evidence that Type 1 quasars violate the Eddington limit by more than a factor of a few.

### 4.4. Completeness in Eddington Ratio

Similar to the calculation performed in Section 3.4, in Figure 14 we show the Eddington ratio at which a survey becomes only 10% complete as a function of redshift for two limiting $i$-band magnitudes. The results are similar for the model with a luminosity-dependent bias. Surveys with a limiting magnitude of $i = 20$ are largely incomplete at $L/L_{\rm Edd} \lesssim 0.07$, while surveys with a limiting magnitude of $i = 24$ start to become severely incomplete at $L/L_{\rm Edd} \lesssim 0.01$. The increase in the completeness limits at $2 < z < 3.2$ mirror other anomalous trends in $L/L_{\rm Edd}$, and the uncertainties are large. As discussed earlier in this work, the SDSS color selection algorithm has difficulty distinguishing quasars from stars in this redshift range, and this may introduce systematic trends with $L/L_{\rm Edd}$. Therefore, we do not consider the "bump" in the completeness limit at $2 < z < 3.2$ to be real. These derived completeness limits are broadly consistent with the lack of Type 1 quasars having $L/L_{\rm Edd} < 0.01$ observed in *COSMOS* by Trump et al. (2011), whose sample starts to become incomplete at $i > 23$.

## 5. DISCUSSION

The results that we have obtained in this work with regard to AGN demographics provide an important window into SMBH growth and AGN fueling, especially when interpreted within the greater context of earlier observational and theoretical work on AGN number densities, clustering, and host galaxy properties. In particular, a picture is emerging in which the fueling mechanisms of SMBH growth are complex and varied. In this section we discuss an interpretation of our results that incorporates other recent observational results; many of the ideas discussed here are treated in greater detail in various theoretical papers (e.g., Hopkins & Hernquist 2006, 2009; Hopkins et al. 2006a, 2008; Croton et al. 2006; Bower et al. 2006; Monaco et al. 2007; Fanidakis et al. 2012).

### 5.1. Black Hole Growth Timescales: Evidence for Self-regulated Growth of SMBHs?

In Figure 15 we show the estimated typical growth time as a function of redshift needed for SMBHs in Type 1 quasars to obtain masses of $M_{\rm BH}/M_\odot = 5 \times 10^8$, $10^9$, $5 \times 10^9$, and $10^{10}$. We estimate the time needed for a SMBH to grow from a seed mass of $M_{\rm seed}$ to a observed mass of $M_{\rm BH}$ at a redshift $z$ as

$$t_{\rm BH} = \frac{t_s}{10\epsilon_r E(L/L_{\rm Edd}|M_{\rm BH}, z)} \ln \frac{M_{\rm BH}}{M_{\rm seed}}, \qquad (20)$$

where $t_s = 4.3 \times 10^7$ yr is the Salpeter ($e$-folding) timescale assuming a radiative efficiency of $\epsilon_r = 0.1$ and $E(L/L_{\rm Edd}|M_{\rm BH}, z)$ is the mean value of $L/L_{\rm Edd}$ at fixed $M_{\rm BH}$ and $z$. We calculated growth timescales assuming a seed mass of $M_{\rm Seed} = 10^6\,M_\odot$ and a radiative efficiency of $\epsilon_r = 0.1$ (e.g., Yu & Tremaine 2002; Davis & Laor 2011). The assumption in these calculations is that the SMBHs in each mass and redshift bin accrete at a time-averaged rate relative to Eddington that is equal to the population average of Type 1 quasars in that bin. While this is not true for every Type 1 quasar in each bin, it should be a good approximation for a representative quasar in each bin; hence the association of these timescales with the "typical" growth time for a SMBH in that bin. In addition, these calculations implicitly assume a duty cycle of unity. For comparison, we also show the age of the universe as a function of $z$. The results were similar for the model with a luminosity-dependent bias,

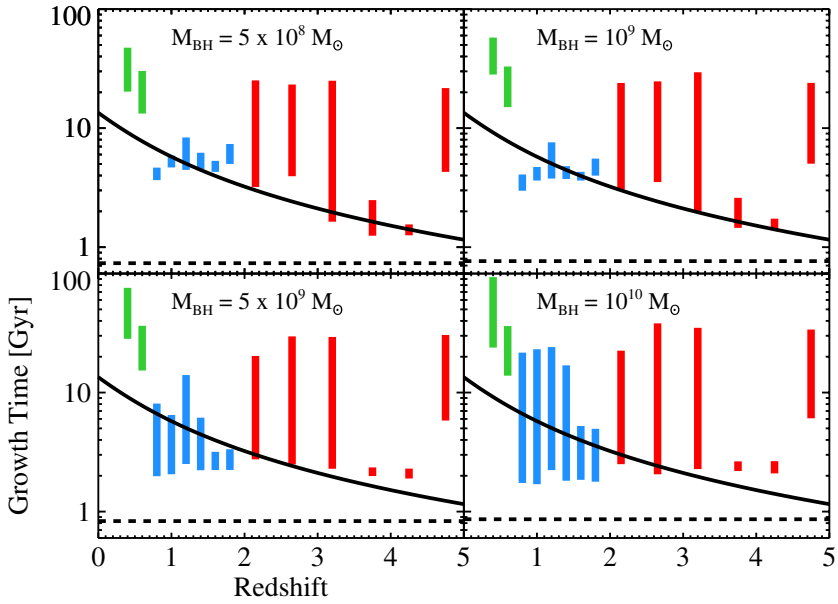


**Figure 15.** Estimated typical time needed for a black hole to grow from a seed mass of $M_{\rm BH}^{\rm seed} = 10^6\,M_\odot$ to four different final masses as a function of redshift, assuming a radiative efficiency of $\epsilon_r = 0.1$ and the typical Eddington ratio for that mass and redshift bin. The solid line marks the age of the universe as a function of $z$, the dashed line marks the growth time assuming $L/L_{\rm Edd} = 1$, and the rest of the labeling is the same as that in Figure 5. Although the uncertainties are large, the growth times for SMBHs in Type 1 quasars having $M_{\rm BH} \gtrsim 5 \times 10^8\,M_\odot$ are comparable to or greater than the age of the universe, suggesting an earlier phase of accelerated obscured growth. The growth times at $z \lesssim 0.6$ are also longer than the age of the universe, possibly reflecting a shift to fueling by mass loss from evolved stellar populations.

(A color version of this figure is available in the online journal.)

but the error bars on the growth times were larger. The value of $\epsilon_r = 0.1$ corresponds to the radiative efficiency of a moderately spinning black hole, and the value of $M_{\rm BH} = 10^6\,M_\odot$ for the seed black holes corresponds to the largest values predicted by models for SMBH seed formation (for a review, see Volonteri 2010). In particular, SMBH seed masses of $M_{\rm BH} = 10^6\,M_\odot$ represent the high end of the distribution predicted from models where SMBH seeds form from the direct collapse of gas (e.g., Volonteri et al. 2008; Volonteri & Begelman 2010; Natarajan & Volonteri 2012).

For many of the mass and redshift bins at $z \gtrsim 2$ the growth times are comparable to or longer than the age of the universe, although the uncertainties are large for several of the bins. If the remnants of Pop-III stars are the SMBH seeds, then values of the seed masses are $M_{\rm BH} \sim 100\,M_\odot$ (e.g., Fryer & Kalogera 2001; Madau & Rees 2001) and the growth times will be a factor of $\sim$2 longer. Similarly, if the black holes are rapidly spinning, as expected from continuous accretion in a disk geometry, then their growth time will be a factor of $\sim$3 longer due to the increased radiative efficiency. In addition, if the duty cycles of Type 1 quasar activity are less than unity, then the growth time will be longer by a factor equal to the inverse of the duty cycle. On the other hand, we have neglected mergers of black holes in these growth times, which may make a non-negligible contribution to shortening the growth times (e.g., Sesana et al. 2007; Tanaka & Haiman 2009). Similarly, if most quasars at high-$z$ host SMBHs are not spinning, the radiative efficiency is $\epsilon_r < 0.1$ and the growth times will be shorter than what we estimate.

Because our estimated typical SMBH growth timescales are comparable to, or longer than, the age of the universe, they imply that many SMBHs underwent an earlier phase of accelerated growth (e.g., with higher Eddington ratio) when we would not have observed them as Type 1 quasars. Similar conclusions have been reached by Netzer et al. (2007), K10, and Trakhtenbrot et al. (2011). It is possible that we do not observe these early rapidly growing SMBHs as Type 1 quasars because they are obscured. Alternatively, it is also possible that the typical Eddington ratio is near unity for Type 1 quasars with masses representative of an earlier phase in their growth (e.g., $M_{\rm BH} \lesssim 5 \times 10^8\,M_\odot$). In this case, we would have missed these rapidly accreting Type 1 quasars because they would have had smaller masses, and therefore would have fallen below our completeness limit. Both possibilities exist but cannot be distinguished by our data.

Our results regarding the growth times of typical SMBHs in Type 1 quasars are in agreement with expectations from models for self-regulated black hole growth (e.g., Sanders et al. 1988; Sanders & Mirabel 1996; Hopkins et al. 2006a). Within the framework of these models, the black hole is enshrouded in material and undergoes Eddington limited obscured growth. The broad-line quasar phase begins after the obscuring material disappears. This can happen because the black hole grows to the point that feedback energy from it becomes powerful enough to "blow" the obscuring material away (e.g., Hopkins et al. 2005, 2006a). Alternatively, the obscuring material may disappear because it becomes consumed by star formation in the bulge. The Type 1 quasar phase is expected to persist until the accretion rate drops low enough to switch to a radiatively inefficient accretion flow (e.g., Churazov et al. 2005; Cao 2005; Shen et al. 2007a; Hopkins et al. 2009). We note that during the blow-out phase there may still be geometry-dependent obscuration caused by a dusty torus, as invoked by the traditional AGN unification models (Antonucci 1993; Urry & Padovani 1995). Our results are therefore consistent with a variety of models for growing the most massive SMBHs at $z \gtrsim 2$, so long as SMBHs exhibited enhanced accretion rates relative to Eddington below $M_{\rm BH} \sim 5 \times 10^8\,M_\odot$.

At redshifts $z \lesssim 0.8$ our calculated black hole growth times are a factor of ~2–3 longer than the age of the universe for SMBHs with $M_{\rm BH} > 5 \times 10^8\,M_\odot$, reflecting the smaller values of $L/L_{\rm Edd}$ at these redshifts. Similar results were obtained by Heckman et al. (2004) and Kauffmann & Heckman (2009) using a sample of low-$z$ Type 2 AGNs. These low-$z$ AGNs likely experienced an earlier stage of rapid growth, and instead we are currently witnessing a reignition of weaker AGN activity reflected in their lower accretion rates and longer growth times. As we discuss below in Section 5.2, the Type 1 quasars probed by our study most likely live in elliptical galaxies, and therefore this low-order AGN activity is probably fueled by stellar mass loss from evolved stars. Although there is little overlap in $M_{\rm BH}$ between the massive systems in our sample and the less massive ones in the sample of Kauffmann & Heckman (2009), at $M_{\rm BH} \sim 3 \times 10^8\,M_\odot$ they derive an Eddington ratio distribution that decreases monotonically toward higher $L/L_{\rm Edd}$, similar to us.

### 5.2. Fueling of SMBHs and Triggering of Type 1 Quasar Activity

Due to incompleteness, our sample probes the Type 1 quasar population with $M_{\rm BH} \gtrsim 3 \times 10^8\,M_\odot$. Locally, SMBHs in this mass range are predominately found in early-type (i.e., elliptical and S0 galaxies) galaxies as inferred from the local SMBH BHMF (Yu & Lu 2004, 2008). This therefore suggests that our study is dominated by SMBHs that currently live in elliptical and S0 host galaxies. Indeed, many studies find that the host galaxies of optically identified AGNs are dominated by early-type galaxies (e.g., Kauffmann et al. 2003; Dunlop et al. 2003; Zakamska et al. 2006; Kotilainen et al. 2007). Currently, the favored mechanism for creating elliptical galaxies is through galaxy mergers (e.g., Springel et al. 2005; Bournaud et al. 2005; Boylan-Kolchin et al. 2006; Cox et al. 2006), suggesting that the Type 1 quasars in our sample have at least in part been fueled by mergers. This is supported by observations that find evidence of past interactions in many local elliptical hosts of quasars (e.g., Bahcall et al. 1997; Bennert et al. 2008). However, we also note that some recent theoretical work suggests that spheroid-dominated galaxies may also form from instabilities in gas-rich disks at high-$z$ (Dekel et al. 2009); furthermore, Bournaud et al. (2011) have argued that AGNs at high-$z$ may form from similar processes. This said, the fraction of galaxies at high-$z$ that contain the massive clumps necessary to form spheroids and AGNs via secular processes is potentially low (Wuyts et al. 2012), and at best unclear.

As discussed above, the typical growth times that we find for $M_{\rm BH} \gtrsim 5 \times 10^8\,M_\odot$ SMBHs in Type 1 quasars at $z \gtrsim 2$ are of order the age of the universe or longer, implying that these SMBHs experienced an earlier phase of accelerated growth. This is expected from models for self-regulated SMBH growth. Such models posit a massive fueling event, such as a major merger, which directs larger amounts of gas toward the nuclear region, fueling obscured Eddington-limited SMBH growth. Eventually, the SMBH's growth is quenched either due to AGN feedback or the consumption of gas due to star formation, revealing the SMBH as a Type 1 quasar and linking the SMBH's final mass with properties of the stellar bulge. Indeed, it is likely that most of our Type 1 quasars currently reside in early-type galaxies, which show the tightest $M_{\rm BH}$–$\sigma^*$ relation (e.g., Gültekin et al. 2009).

Due to incompleteness our sample only probes SMBHs with $M_{\rm BH} \gtrsim 3 \times 10^8\,M_\odot$, and it is unlikely that our results and discussion extend to lower mass SMBHs. Estimates of the local BHMF for all SMBHs imply that late types should dominate SMBH-host galaxies below $5 \times 10^7\,M_\odot$ (e.g., Yu & Lu 2004, 2008). Furthermore, among galaxies that have been used to define the $M_{\rm BH}$–$\sigma_*$ relationship, late types are found at $M_{\rm BH} \lesssim 10^8\,M_\odot$ (e.g., McConnell et al. 2011). Many recent studies of X-ray-selected AGNs at lower luminosities ($L_{\rm bol} <$ a few $\times\ 10^{45}$ erg s$^{-1}$) have found that AGNs live in both bulge- and disk-dominated galaxies out to $z \sim 2$, and that their host galaxies are no more likely to show evidence of disturbances or interaction signatures than their inactive counterparts (Grogin et al. 2005; Pierce et al. 2007; Gabor et al. 2009; Cisternas et al. 2011; Schawinski et al. 2011; Pović et al. 2012; Kocevski et al. 2012, but see Koss et al. 2010). However, it should be noted that there are difficulties in identifying mergers as the trigger of AGN activity due to a possible time-lag between the merger and the initiation of AGN activity (e.g., Hopkins et al. 2006b; Schawinski et al. 2010), combined with the rapid fading of the morphological features indicative of a recent merger (Lotz et al. 2010).

Studies of AGN host galaxy colors have found results consistent with the morphology studies: namely, that AGNs live in both early- and late-type galaxies (e.g., Nandra et al. 2007; Coil et al. 2009; Silverman et al. 2009; Schawinski et al. 2009; Xue et al. 2010; Georgakakis et al. 2011). The most recent studies are able to go deeper and find a higher fraction of AGNs in disk galaxies. Indeed, Kocevski et al. (2012) found a correlation between X-ray luminosity and the fraction of AGNs in spheroidal galaxies, and Treister et al. (2012) found a correlation between AGN luminosity and the fraction of host galaxies undergoing a major merger. These results suggest that AGNs with more massive SMBHs tend to be found in early types and fueled by major mergers even out to $z \sim 2$–3. However, the larger fraction of AGNs with less massive SMBHs in disk galaxies suggests that these SMBHs are grown through processes other than a major merger up to the point that we observe them, and it is unclear if they also experience an earlier phase of accelerated growth. Moreover, the weaker $M_{\rm BH}$–$\sigma_*$ relationship for late-type galaxies (e.g., Graham 2008; Gültekin et al. 2009; Greene et al. 2010b; Kormendy et al. 2011) suggests that the growth of these SMBHs is more weakly coupled to the evolution of the host galaxy, if any relationship exists at all. In contrast, the more massive SMBHs ($M_{\rm BH} \gtrsim 3 \times 10^8\,M_\odot$) probed by our Type 1 quasar sample are grown through a process that also generates a spheroid and places the SMBH on the local $M_{\rm BH}$–$\sigma_*$ relation, with a major merger of two gas-rich galaxies likely being the dominant fueling mechanism.

### 5.3. Downsizing of SMBHs and Duty Cycles of Type 1 Quasar Activity

In this work we have also found evidence for downsizing in both $M_{\rm BH}$ and $L/L_{\rm Edd}$. The downsizing in $M_{\rm BH}$ is consistent with results from SMBHs in Type 1 quasars (e.g., Vestergaard et al. 2008; Labita et al. 2009a; K10; Paper I) and for the entire SMBH population as derived from the continuity equation methods (e.g., Marconi et al. 2004; Merloni 2004), and reflects the fact that the most massive SMBHs tended to experience active phases and the bulk of their growth before less massive SMBHs. Studies of AGN clustering have concluded that AGNs are observed to reside in dark matter halos of $M_h \sim 3 \times 10^{12}\,M_\odot$ at all redshifts (e.g., Porciani et al. 2004; Croom et al. 2005; Coil et al. 2007; Myers et al. 2007; Shen et al. 2007b, 2009; Ross et al. 2009; da Ângela et al. 2008; Mandelbaum et al. 2009; Hickox

et al. 2009, 2011; White et al. 2012). The combination of the clustering results and AGN downsizing led Hickox et al. (2009) to argue that AGN activity is triggered when a SMBH's host halo reaches $M_h \sim 3 \times 10^{12}\,M_\odot$, and that the observed downsizing in $M_{\rm BH}$ is a reflection of the fact that the most massive SMBHs in the present epoch are those that resided in the most massive halos at high redshift, and these are the halos that reached a critical mass of $M_h \sim 3 \times 10^{12}\,M_\odot$ first.

We can also use our estimated Type 1 quasar BHMF to estimate the duty cycle for Type 1 quasar activity. We estimate the duty cycle at $z \sim 0.4$ and $z \sim 1.0$ for Type 1 quasar activity of SMBHs with $M_{\rm BH} = 10^9\,M_\odot$ by taking the ratio of our estimated BHMF to the local BHMF for all SMBHs at $M_{\rm BH} = 10^9\,M_\odot$, where the local BHMF and its uncertainty are taken from the compilation of Shankar et al. (2009b). The local BHMF should provide a good estimate of the BHMF at $z = 0.4$ and $z = 1.0$ as the bulk of the BHMF at $M_{\rm BH} \sim 10^9\,M_\odot$ was already in place by $z \sim 1$ (e.g., Merloni & Heinz 2008). We find duty cycles of $6.0^{+3.9}_{-2.4} \times 10^{-3}$ and $9.1^{+3.8}_{-2.7} \times 10^{-3}$ (68% credibility intervals) for $M_{\rm BH} = 10^9\,M_\odot$ at $z = 0.4$ and $z = 1$, respectively. Similarly, we also estimate the duty cycle of Type 1 quasar activity for $M_{\rm BH} = 10^9\,M_\odot$ SMBHs at $z = 2$ by comparing with the BHMF for all SMBHs derived from continuity equations methods. Comparing our active BHMF with the compilation of $z = 2$ BHMFs shown in Figure 7(b) of Kelly & Merloni (2012), we estimate the $z = 2$ duty cycle of Type 1 quasar activity to be $> 0.06$. These results show that for SMBHs with $M_{\rm BH} \sim 10^9\,M_\odot$ Type 1 quasar activity is a rare and likely short-lived phenomenon, and was more common at higher redshift, implying that the massive end of the BHMF was built up primarily at early times. Similar results were obtained in Paper I by comparing the cumulative mass densities in Type 1 Quasars with all SMBHs.

The duty cycles that we estimate are broadly consistent with those derived from continuity models by Shankar et al. (2013) for their Gaussian + Power-law Eddington ratio model. Moreover, the $z = 1$ duty cycle that we estimate is very similar to that estimated by K10 from the SDSS DR3, and our estimated duty cycle at $z = 0.4$ is about an order of magnitude larger than that at $z < 0.3$ estimated by Schulze & Wisotzki (2010). This latter point implies that the duty cycle of Type 1 quasar activity for $M_{\rm BH} = 10^9\,M_\odot$ SMBHs declines rapidly from $z \sim 0.4$. However, we also note that our $z \sim 0.4$ duty cycle may also be overestimated due to a bias in our incompleteness correction caused by unaccounted for host galaxy flux in the SDSS selection function, as discussed in Sections 3.2 and 5.6. And finally, our estimated growth times at high redshift imply duty cycles of order unity, as it is difficult to accommodate the longer growth times required by smaller values of the duty cycle given that the estimated growth timescales are already comparable to the age of the universe at these redshifts. Our inferred large duty cycles for luminous quasars at high redshift are consistent with the large duty cycles inferred by quasar clustering measurements at $z \gtrsim 3$ (e.g., White et al. 2008; Shankar et al. 2010; Shen et al. 2010; Bonoli et al. 2010).

### 5.4. Eddington Ratio Distributions and Type 1 Quasar Lightcurves

Under self-regulated growth models, during the Type 1 quasar phase the AGN lightcurve exhibits a power-law-like decay, either due to the decrease in the fueling rate due to evolution of a feedback-driven blast wave (Hopkins & Hernquist 2006) or due to viscous evolution of an accretion disk resulting from a quenched fuel supply (e.g., Yu et al. 2005; King & Pringle 2007). If the AGN lightcurve is decaying during the Type 1 quasar phase, then we would expect a broad range of Eddington ratios with the number densities increasing monotonically toward lower values of $L/L_{\rm Edd}$. This is consistent with our estimated BHERF, although we note that predictions for this type of BHERF are not unique to self-regulated black hole growth models.

Our estimated BHERF is consistent with the $z \sim 1.4$ BHERF derived by Nobuta et al. (2012) from a much deeper sample of X-ray-selected Type 1 quasars. In addition, our BHERF is qualitatively consistent with the results of Aird et al. (2012) and Bongiorno et al. (2012). These authors found that the distribution of X-ray luminosity at fixed stellar mass exhibits a power-law-like increase toward fainter X-ray luminosities for Type 2 quasars (in the case of Aird et al. 2012) and both Type 1 and Type 2 quasars (in the case of Bongiorno et al. 2012). Because $M_{\rm BH}$ is correlated with stellar mass (e.g., Magorrian et al. 1998; Häring & Rix 2004), the results of Aird et al. (2012) and Bongiorno et al. (2012) imply that the number densities of active SMBHs increase toward lower Eddington ratio. This is in agreement with our estimated marginal distribution of Eddington ratio, i.e., the BHERF. However, these authors also concluded that the power-law distribution of X-ray luminosity at fixed stellar mass is the same for all stellar mass bins. This is inconsistent with our result that for some of the redshift bins the distribution of Eddington ratio changes with $M_{\rm BH}$. That being said, the relationship between $M_{\rm BH}$ and stellar mass is complex and exhibits statistical scatter (Graham 2012), making a quantitative comparison of our results (which are with respect to $M_{\rm BH}$) with those of Aird et al. (2012) and Bongiorno et al. (2012; which are respect to stellar mass) difficult. Moreover, both the Aird et al. (2012) and Bongiorno et al. (2012) samples are X-ray selected and contain Type 2 quasars, and thus may probe a different population of objects. Thus, is it unclear how inconsistent our results are compared with theirs. In addition, the broad Eddington ratio distributions that we find at $z > 3$ may be inconsistent with small scatter in the $L$–$M_h$ relation inferred from clustering measurements (e.g., White et al. 2008; Shankar et al. 2010; Shen et al. 2010; Bonoli et al. 2010). It is unclear how to reconcile these results, especially if $M_{\rm BH}$ and $M_h$ are strongly correlated.

In addition, we have found that the distribution of $L/L_{\rm Edd}$ is either approximately independent of $M_{\rm BH}$ or shifts to larger values with increasing $M_{\rm BH}$, depending on the redshift bin, in contrast to the results from continuity equation techniques (Shankar et al. 2013) or from theoretical models (e.g., Granato et al. 2004; Lapi et al. 2006). Part of this discrepancy may be that we only analyze the joint distribution of $M_{\rm BH}$ and $L/L_{\rm Edd}$ for Type 1 quasars, while other techniques tend to focus on the entire AGN population. This behavior could represent a real effect, possibly due to evolution in the Type 1 quasar lightcurve caused by, for example, a shallower decay in accretion rate at $1 \lesssim z \lesssim 3$ during the blow-out phase for more massive SMBHs. However, as discussed in Section 5.6 there are several systematics that complicate analysis of the joint distribution of Type 1 quasars in the mass luminosity plain, including a possible dependence of the bolometric correction on $M_{\rm BH}$ or $L/L_{\rm Edd}$ and unknown systematic errors in the virial mass estimates for Mg II and C IV. In addition, the continuity equation methods are also potentially affected by systematics as discussed in Kelly & Merloni (2012). Considering this, it is unclear whether the dependence of the Eddington ratio distribution on $M_{\rm BH}$ that we find is real, and

these discrepancies highlight the need for further improvement in our understanding of the virial mass estimates, bolometric corrections, and extensions of AGN demographical studies to deeper surveys.

The downsizing in $L/L_{\rm Edd}$ has a somewhat different form than that of $M_{\rm BH}$. Unlike the number densities of $M_{\rm BH}$, the number densities in bins of constant $L/L_{\rm Edd}$ do not show any evolution at $z < 2$. Instead, we observed "downsizing" in $L/L_{\rm Edd}$ in the sense that Type 1 quasars radiating at $L/L_{\rm Edd} \lesssim 0.1$ are significantly more rare at $z \sim 4$ compared with $z \lesssim 2$, while the number densities of Type 1 quasars at $L/L_{\rm Edd} \gtrsim 0.1$ are similar for $z \sim 2$ and $z \sim 4$. This may reflect a stronger contribution to the BHERF at $z \sim 2$ from Type 1 quasars that are further along the decaying part of the AGN lightcurve, and thus at a lower $L/L_{\rm Edd}$, possibly due to a more prolonged post-peak phase. In addition, this change in the $L/L_{\rm Edd}$ distribution at $z \lesssim 3$ may reflect a stronger contribution of Type 1 quasars that are fueled through more internal processes and experiencing weaker AGN activity. However, because our sample becomes significantly incomplete below $L/L_{\rm Edd} \lesssim 0.07$ it is unclear how significant this trend is.

Based on our derived BHERF, we conclude that those Type 1 quasars that do radiate near the Eddington limit are extremely rare, suggesting that if Type 1 quasars do violate the Eddington limit they do so only for a very brief period of time. In such supercritical accretion flows the luminosity depends logarithmically on the accretion rate, so in principle these Type 1 quasars that do radiate at $L/L_{\rm Edd} > 1$ could be accreting at a significantly higher rate relative to Eddington, i.e., $\dot{M}/\dot{M}_{\rm Edd} \gg 1$.

### 5.5. Comparison with Models for SMBH Growth

Direct comparison of our results with models of SMBH fueling and growth is difficult, as most models do not present a quantitative prediction of the BHMF and BHERF specifically for Type 1 quasars. Instead, many modelers predict the BHMF and BHERF for all SMBHs, or for active SMBHs. Generically, many models predict a BHMF that increases toward lower mass down to $M_{\rm BH} \lesssim 3 \times 10^8\,M_\odot$, which is in agreement with our estimated BHMF. In addition, many models predict downsizing in SMBH growth and AGN activity, in agreement with our empirical results. Natarajan & Volonteri (2012) compared BHMFs for Type 1 quasars with models for merger driven SMBH growth that assumed that either SMBH seeds are the remnants of Pop-III stars or were formed through direct collapse of pre-galactic disks (Lodato & Natarajan 2007). They compared their model unobscured quasar BHMF to those estimated by K10, and in general they found that the Pop-III seeding model underpredicted the BHMF at $M_{\rm BH} \gtrsim 10^9\,M_\odot$. Their direct collapse seeding model provided a better fit at $z < 4$, although it overpredicts the number densities of the most massive SMBHs in Type 1 quasars at $z \lesssim 2$; however, the authors argue that the overprediction is not a problem, as it results from the fact that they did not implement depletion of the available gas to grow the SMBH at lower $z$. None of their models were able to match the K10 BHMF at $z = 4.25$. Because the K10 BHMF was derived from the SDSS DR3, which is a subset of our sample, it is not greatly different from the BHMF that we derive here. As such, the conclusions reached by Natarajan & Volonteri (2012) would be unchanged using our newer BHMF, although we note that comparison with our new BHMF implies that all of their models underpredict our derived number densities of SMBHs in Type 1 quasars with $M_{\rm BH} \sim 3 \times 10^8\,M_\odot$ at $z = 1.25$.

The most massive SMBHs in the observable universe implied by our BHMF have masses $10^{10}\,M_\odot$–$10^{11}\,M_\odot$, consistent with earlier results obtained by K10. However, as this value is strongly dependent on our prior for the extreme high mass tail of the BHMF, a more realistic constraint is $M_{\rm BH}^{\rm max} \gtrsim 10^{10}\,M_\odot$. Recently McConnell et al. (2011) detected two SMBHs in the local universe with $M_{\rm BH} \sim 10^{10}\,M_\odot$ determined from stellar dynamical modeling. Considering the different volumes probed by the SDSS DR7 and their search, their results are consistent with the limits on the maximum mass implied by our BHMF. In addition, the lower limits on the maximum masses that we infer are consistent with values predicted from models that assume the SMBH's growth is self-regulated (Natarajan & Treister 2009). Simulations that follow the growth of SMBHs in bright $z \sim 6$ quasars have also been able to grow SMBHs to $M_{\rm BH} \sim 2 \times 10^{10}\,M_\odot$ by $z \sim 2$ (Sijacki et al. 2009).

### 5.6. Sources of Systematic Error

While we have obtained a number of interesting results, there are a few caveats regarding our approach that must be kept in mind, and we conclude this section with a discussion of them. There are three significant potential sources of systematic error in our approach, which we have touched on earlier: incorrect specification of the virial mass error distribution and bias, errors in the SDSS selection function, and errors in the bolometric correction. In this work we have used a simple constant bolometric correction to the 2500 Å luminosity, and, strictly speaking, our derived BHERF should be viewed as the number density of Type 1 quasars radiating at a given ratio of optical luminosity to Eddington, scaled upward by a constant factor of five. Because the bolometric correction likely depends on both $M_{\rm BH}$ and $L/L_{\rm Edd}$, this will create systematic errors. It is unclear how these systematics in the bolometric correction affect our results on the BHERF. In principle it is possible to incorporate a variable bolometric correction into our Bayesian model, but unfortunately there is considerable uncertainty in the distribution of bolometric corrections as a function of $M_{\rm BH}$ and $L/L_{\rm Edd}$.

As discussed in Sections 3.2 and 4.1 systematic errors on the selection function can have a significant effect on our results in highly incomplete regions of parameter space. In general we have limited our analysis to masses or Eddington ratios in which we are not highly incomplete (i.e., completeness $\gtrsim$10%), so we do not expect small errors in the selection function to have a significant effect on our results. However, this is not true in the redshift bins corresponding to $z = (2.15, 2.65, 3.20)$. In these bins the SDSS selection algorithm has difficulty distinguishing quasars from stars, and as a result these bins are highly incomplete. Moreover, the distribution of quasar colors obtained from the simulations used to estimate the selection function do not perfectly match the observed distributions, and the selection algorithm is color dependent at these redshifts. We do not include a color dependence in the selection function, and, because the quasar SED depends on $M_{\rm BH}$ and $L/L_{\rm Edd}$, this likely introduces systematic errors into our incompleteness correction. Because of this the BHMF and BHERF derived at these redshifts should be interpreted with caution.

The most important possible source of systematic error in our approach arises from incorrectly specifying the error distribution of the virial mass estimates. This is particularly a concern for Mg II and C IV, which are not as well studied with respect to the reverberation mapping database as H$\beta$. In addition, C IV emission is thought to at least partly arise from an accretion

disk wind and may contain a non-virial component to the line width (e.g., Shen et al. 2008; Richards et al. 2011), although it is currently unclear whether this creates a significant bias in the C IV-based mass estimates. We have tried to incorporate some systematic errors resulting from a bias in the virial mass estimates to the extant that it can be modeled as having a simple luminosity dependence. There were no significant differences in our main scientific conclusions when we included a simple luminosity-dependent bias. In addition, we have tried to mitigate the affects of some objects having large systematic errors in the mass estimates through our use of a Student's $t$-distribution as a model for the measurement errors on the mass estimates, which downweights any outliers.

In general, the number densities of the virial mass estimates obtained before correcting for incompleteness do not show discontinuities across redshift bins when switching emission lines (Paper I). However, there are a few discontinuities in the derived mass and Eddington ratio functions when switching between emission lines, suggesting that small systematics between the virial mass estimates of different emission lines may be manifested more strongly in our derived BHMF and BHERF. These include a discontinuity in the normalization of the BHMF when going from H$\beta$ to Mg II (Figure 5), a discontinuity in the BHERF when going from Mg II to C IV (Figure 10), and differences in the distribution of $L/L_{\rm Edd}$ at fixed $M_{\rm BH}$ inferred from the three emission lines (Figure 12). While it may be tempting to conclude from this that one or more of the emission lines do not give consistent results, this is not necessarily the case. As discussed in Section 3.2, the increase in number densities in the redshift bins using H$\beta$ is likely at least in part caused by a host-galaxy contribution to the nuclear emission that is not accounted for in the selection function, creating an excess of AGNs in these redshift bins as their nuclear emission gets boosted above the flux limit. The discontinuity in the number densities across $z \sim 2$, corresponding to the shift from Mg II to C IV, also corresponds to a transition in the selection function to redshifts where quasar colors are similar to star colors. As discussed above and in Section 4.1 this can lead to significant systematic error in the incompleteness correction; indeed, these redshift bins have the largest statistical errors as well.

The only systematic differences between the emission lines in the inferred distribution that cannot be explained as systematics from incorrect incompleteness correction is the anomalous behavior of the Eddington ratio distribution at fixed $M_{\rm BH}$. The distribution of $L/L_{\rm Edd}$ is independent of $M_{\rm BH}$ for the two bins employing H$\beta$, shifts toward larger values of $L/L_{\rm Edd}$ with increasing $M_{\rm BH}$ for the redshift bins employing Mg II, and then shifts to being independent of $M_{\rm BH}$ again over the redshift bins employing C IV. Although it has been argued that C IV is less reliable than Mg II or H$\beta$ (e.g., Baskin & Laor 2005; Shen et al. 2008; Shen & Liu 2012), in this case it is Mg II that gives the discrepant result. It is unclear why this is the case, and it may be that this observed trend represents real evolution in the joint distribution of $M_{\rm BH}$ and $L/L_{\rm Edd}$. However, we consider it likely that unidentified systematics are at least in part driving this trend. Because of this, our current understanding of virial mass estimates may not provide enough accuracy for inferring how percentiles of the Type 1 quasar joint distribution vary in the mass–luminosity plane.

## 6. SUMMARY

In this work we have employed a Bayesian analysis method to derive the black hole mass and Eddington ratio functions for broad-line AGNs using a uniformly selected sample from the SDSS DR7. We used more flexible models than those in Paper I to test the robustness of the key conclusions of Paper I, and found that the main results in Paper I remain valid, although the constraints are weakened due to the more flexible models used in the current work. Our conclusions are summarized as follows.

1. The SDSS is $\lesssim$10% complete at $M_{\rm BH} \lesssim 3 \times 10^8\,M_\odot$ or $L/L_{\rm Edd} \lesssim 0.07$, with some variation with redshift. Decreasing the magnitude limits to $i \sim 24$, similar to that of the *COSMOS* spectroscopic surveys or the *Pan-STARRS* medium-deep fields, reduces the mass and Eddington ratio incompleteness limits by about an order of magnitude.
2. There is a broad range of $M_{\rm BH}$ and $L/L_{\rm Edd}$ for Type 1 quasars, and there is no evidence for a peak in the black hole mass or Eddington ratio functions down to the 10% completeness limits of the SDSS sample. The number densities of Type 1 quasars continue to increase toward lower $M_{\rm BH}$ and $L/L_{\rm Edd}$ down to at least $M_{\rm BH} \sim 5\times10^8\,M_\odot$ and $L/L_{\rm Edd} \sim 0.07$, respectively.
3. Both the BHMF and BHERF show evidence for downsizing. Relative to the peak in the number densities at $z \sim 2$, the number densities of the most massive black holes in Type 1 quasars fall off fastest toward lower redshift, while the number densities of the less massive black holes fall off faster toward higher $z$. This implies that the most massive black holes were active first, and shut off their activity more rapidly after the peak.
   The number densities of Type 1 quasars are approximately constant at $z \lesssim 2$ for $L/L_{\rm Edd} \gtrsim 0.05$; however, the number densities of Type 1 quasars radiating at $L/L_{\rm Edd} \lesssim 0.1$ fall off more rapidly toward higher redshift at $z \gtrsim 2$, possibly reflecting a smaller contribution from weaker AGN activity toward higher redshift.
4. We constrain the maximum value of $L/L_{\rm Edd}$ in a Type 1 quasar to be $\sim$3. Therefore, if quasars do violate the Eddington limit, they do so only mildly and for a short period of time.
5. At low ($z \lesssim 0.8$) and high ($z \gtrsim 2.65$) redshifts the Eddington ratio distribution at fixed $M_{\rm BH}$ is approximately independent of $M_{\rm BH}$. However, at redshifts $0.8 \lesssim z \lesssim 2.65$ $p(L/L_{\rm Edd}|M_{\rm BH})$ shifts toward higher values of $L/L_{\rm Edd}$ from $M_{\rm BH} = 5 \times 10^8\,M_\odot$ to $M_{\rm BH} = 5 \times 10^9\,M_\odot$. This therefore implies that at intermediate redshifts the shape of the Eddington ratio distribution changes such that the high $L/L_{\rm Edd}$ tail becomes more dominant at higher $M_{\rm BH}$. At low and high-$z$ the shape of the high $L/L_{\rm Edd}$ tail of the Eddington ratio distribution is independent of $M_{\rm BH}$. The redshift dependence of this trend is unexpected and may be due to unidentified systematics among the emission lines used to calculate the FWHM-based virial mass estimates.
6. We do not find statistical evidence for the so-called sub-Eddington boundary in the quasar mass–luminosity plane claimed by Steinhardt & Elvis (2010a). The appearance of such a boundary in the "observed" distribution is caused by selection effects and errors in the virial BH mass estimates (Paper I). This reinforces our early conclusions in Paper I that one should not interpret the observed distribution directly.
7. Assuming a radiative efficiency of $\epsilon_r = 0.1$ and a seed black hole mass of $M_{\rm BH} = 10^6\,M_\odot$, the growth times for SMBHs in Type 1 quasars having $M_{\rm BH} \gtrsim 5 \times 10^8\,M_\odot$

are comparable to or longer than the age of the universe at $z \gtrsim 1.8$. Here, the growth times were calculated assuming that SMBHs in a given mass bin accrete at a time-averaged rate that is equal to the mean Eddington ratio in that mass bin. These large growth times imply that prior to us observing them as Type 1 quasars, these SMBHs experienced a stage of accelerated growth (i.e., with higher Eddington ratios).

8. Comparison of the $M_{\rm BH}$ completeness limits of our sample with the local mass function of all SMBHs implies that our sample is dominated by SMBHs representing the high mass end of the BHMF, which reside in what are locally early-type galaxies. This conclusion in combination with our results on SMBH growth times is consistent with models by which SMBHs experience a massive fueling event which initiates obscured growth. The black hole's growth is self-regulated, persisting until either feedback energy unbinds the obscuring gas or all of the gas is consumed from star formation, briefly revealing the massive black hole as a Type 1 quasar with a decaying lightcurve. This same fueling event leaves behind a spheroid, placing the SMBH on the $M_{\rm BH}$–$\sigma_*$ relationship. Because the SMBHs in our sample represent the high mass end of BHMF, this process may only be common among this mass range. In addition, the long growth times of $z \lesssim 0.8$ Type 1 quasars with massive BHs and low Eddington ratios likely represent weaker AGN activity reignited by mass loss from evolved stellar populations.

The combination of our large uniformly selected sample with our powerful Bayesian method represents an important contribution to AGN demographic studies, and we have used our sample and method in a two-paper series to obtain constraints on the optical luminosity function, BHMF, and BHERFs of Type 1 quasars. In addition, we have used our sample and method to place constraints on the distribution and biases of the virial mass estimates. The results and methods presented in Paper I and in this paper represent important empirical tools for understanding black hole growth, for comparison to theoretical models, and for planning future surveys. In many ways systematic AGN demographic studies with respect to $M_{\rm BH}$ and $L/L_{\rm Edd}$ are just beginning. Further improvement will result from using future reverberation mapping campaigns to refine our understanding of virial mass estimators, as well as applying methods similar to our Bayesian technique to current and future deeper surveys with possibly multiwavelength data.

We thank Desika Narayanan, Marta Volonteri, and Benny Trakhtenbrot for helpful discussions, and Marianne Vestergaard, Tommaso Treu, Priya Natarajan, Marta Volonteri, Andreas Schulze, and Alister Graham for helpful comments on drafts of our manuscript. We also thank the anonymous referee for comments that helped improve our clarity, focus, and discussion. B.C.K. acknowledges support from the Southern California Center for Galaxy Evolution, a multi-campus research program funded by the University of California Office of Research. Y.S. acknowledges support from the Smithsonian Astrophysical Observatory (SAO) through a Clay Postdoctoral Fellowship.

Funding for the SDSS and SDSS-II has been provided by the Alfred P. Sloan Foundation, the Participating Institutions, the National Science Foundation, the U.S. Department of Energy, the National Aeronautics and Space Administration, the Japanese Monbukagakusho, the Max Planck Society, and the Higher Education Funding Council for England. The SDSS Web site is http://www.sdss.org/.

*Facility:* Sloan

## REFERENCES

Aird, J., Coil, A. L., Moustakas, J., et al. 2012, ApJ, 746, 90
Aird, J., Nandra, K., Laird, E. S., et al. 2010, MNRAS, 401, 2531
Aller, M. C., & Richstone, D. 2002, AJ, 124, 3035
Aller, M. C., & Richstone, D. O. 2007, ApJ, 665, 120
Alonso, M. S., Lambas, D. G., Tissera, P., & Coldwell, G. 2007, MNRAS, 375, 1017
Antonucci, R. 1993, ARA&A, 31, 473
Babić, A., Miller, L., Jarvis, M. J., et al. 2007, A&A, 474, 755
Bahcall, J. N., Kirhakos, S., Saxe, D. H., & Schneider, D. P. 1997, ApJ, 479, 642
Barger, A. J., Cowie, L. L., Mushotzky, R. F., et al. 2005, AJ, 129, 578
Baskin, A., & Laor, A. 2005, MNRAS, 356, 1029
Begelman, M. C., & Nath, B. B. 2005, MNRAS, 361, 1387
Bennert, N., Canalizo, G., Jungwiert, B., et al. 2008, ApJ, 677, 846
Bennert, V. N., Treu, T., Woo, J.-H., et al. 2010, ApJ, 708, 1507
Bentz, M. C., Peterson, B. M., Netzer, H., Pogge, R. W., & Vestergaard, M. 2009a, ApJ, 697, 160
Bentz, M. C., Walsh, J. L., Barth, A. J., et al. 2009b, ApJ, 705, 199
Bongiorno, A., Merloni, A., Brusa, M., et al. 2012, MNRAS, 427, 3103
Bongiorno, A., Zamorani, G., Gavignaud, I., et al. 2007, A&A, 472, 443
Bonning, E. W., Cheng, L., Shields, G. A., Salviander, S., & Gebhardt, K. 2007, ApJ, 659, 211
Bonoli, S., Shankar, F., White, S. D. M., Springel, V., & Wyithe, J. S. B. 2010, MNRAS, 404, 399
Bournaud, F., Dekel, A., Teyssier, R., et al. 2011, ApJL, 741, 33
Bournaud, F., Jog, C. J., & Combes, F. 2005, A&A, 437, 69
Bower, R. G., Benson, A. J., Malbon, R., et al. 2006, MNRAS, 370, 645
Boylan-Kolchin, M., Ma, C.-P., & Quataert, E. 2006, MNRAS, 369, 1081
Boyle, B. J., Shanks, T., Croom, S. M., et al. 2000, MNRAS, 317, 1014
Cao, X. 2005, ApJL, 631, 101
Cao, X. 2010, ApJ, 725, 388
Cattaneo, A., Blaizot, J., Devriendt, J., & Guiderdoni, B. 2005, MNRAS, 364, 407
Churazov, E., Sazonov, S., Sunyaev, R., et al. 2005, MNRAS, 363, L91
Ciotti, L., & Ostriker, J. P. 1997, ApJL, 487, 105
Ciotti, L., & Ostriker, J. P. 2007, ApJ, 665, 1038
Cisternas, M., Jahnke, K., Inskip, K. J., et al. 2011, ApJ, 726, 57
Coil, A. L., Georgakakis, A., Newman, J. A., et al. 2009, ApJ, 701, 1484
Coil, A. L., Hennawi, J. F., Newman, J. A., Cooper, M. C., & Davis, M. 2007, ApJ, 654, 115
Collin, S., Kawaguchi, T., Peterson, B. M., & Vestergaard, M. 2006, A&A, 456, 75
Cox, T. J., Dutta, S. N., Di Matteo, T., et al. 2006, ApJ, 650, 791
Cowie, L. L., Barger, A. J., Bautz, M. W., Brandt, W. N., & Garmire, G. P. 2003, ApJL, 584, 57
Croom, S. M., Boyle, B. J., Shanks, T., et al. 2005, MNRAS, 356, 415
Croom, S. M., Richards, G. T., Shanks, T., et al. 2009, MNRAS, 399, 1755
Croton, D. J., Springel, V., White, S. D. M., et al. 2006, MNRAS, 365, 11
Czerny, B., Różańska, A., & Kuraszkiewicz, J. 2004, A&A, 428, 39
da Ângela, J., Shanks, T., Croom, S. M., et al. 2008, MNRAS, 383, 565
Davis, S. W., & Laor, A. 2011, ApJ, 728, 98
Decarli, R., Falomo, R., Treves, A., et al. 2010, MNRAS, 402, 2453
DeGraf, C., Di Matteo, T., Khandai, N., & Croft, R. 2012, ApJL, 755, 8
Dekel, A., Sari, R., & Ceverino, D. 2009, ApJ, 703, 785
Denney, K. D., Peterson, B. M., Dietrich, M., Vestergaard, M., & Bentz, M. C. 2009, ApJ, 692, 246
Di Matteo, T., Colberg, J., Springel, V., Hernquist, L., & Sijacki, D. 2008, ApJ, 676, 33
Di Matteo, T., Springel, V., & Hernquist, L. 2005, Natur, 433, 604
Draper, A. R., & Ballantyne, D. R. 2012, ApJ, 751, 72
Dunlop, J. S., McLure, R. J., Kukula, M. J., et al. 2003, MNRAS, 340, 1095
Ellison, S. L., Patton, D. R., Mendel, J. T., & Scudder, J. M. 2011, MNRAS, 418, 2043
Fabian, A. C. 1999, MNRAS, 308, L39
Fan, X., Hennawi, J. F., Richards, G. T., et al. 2004, AJ, 128, 515
Fan, X., Strauss, M. A., Schneider, D. P., et al. 2001, AJ, 121, 54
Fanidakis, N., Baugh, C. M., Benson, A. J., et al. 2011, MNRAS, 410, 53
Fanidakis, N., Baugh, C. M., Benson, A. J., et al. 2012, MNRAS, 419, 2797
Fine, S., Croom, S. M., Hopkins, P. F., et al. 2008, MNRAS, 390, 1413
Fiore, F., Puccetti, S., Grazian, A., et al. 2012, A&A, 537, A16

Fontanot, F., Cristiani, S., Monaco, P., et al. 2007, A&A, 461, 39
Fryer, C. L., & Kalogera, V. 2001, ApJ, 554, 548
Gabor, J. M., Impey, C. D., Jahnke, K., et al. 2009, ApJ, 691, 705
García-Burillo, S., Combes, F., Schinnerer, E., Boone, F., & Hunt, L. K. 2005, A&A, 441, 1011
Gavignaud, I., Wisotzki, L., Bongiorno, A., et al. 2008, A&A, 492, 637
Gebhardt, K., Bender, R., Bower, G., et al. 2000, ApJL, 539, 13
Gelman, A., Meng, X. L., & Stern, H. S. 1996, Statistica Sinica, 6, 733
Georgakakis, A., Coil, A. L., Willmer, C. N. A., et al. 2011, MNRAS, 418, 2590
Graham, A. W. 2008, ApJ, 680, 143
Graham, A. W. 2012, ApJ, 746, 113
Graham, A. W., & Driver, S. P. 2007, ApJ, 655, 77
Graham, A. W., Erwin, P., Caon, N., & Trujillo, I. 2001, ApJL, 563, 11
Graham, A. W., Onken, C. A., Athanassoula, E., & Combes, F. 2011, MNRAS, 412, 2211
Granato, G. L., De Zotti, G., Silva, L., Bressan, A., & Danese, L. 2004, ApJ, 600, 580
Greene, J. E., & Ho, L. C. 2007, ApJ, 667, 131
Greene, J. E., Hood, C. E., Barth, A. J., et al. 2010a, ApJ, 723, 409
Greene, J. E., Peng, C. Y., Kim, M., et al. 2010b, ApJ, 721, 26
Grogin, N. A., Conselice, C. J., Chatzichristou, E., et al. 2005, ApJL, 627, 97
Gültekin, K., Richstone, D. O., Gebhardt, K., et al. 2009, ApJ, 698, 198
Haiman, Z., & Loeb, A. 2001, ApJ, 552, 459
Häring, N., & Rix, H.-W. 2004, ApJL, 604, 89
Hasinger, G., Miyaji, T., & Schmidt, M. 2005, A&A, 441, 417
Heckman, T. M., Kauffmann, G., Brinchmann, J., et al. 2004, ApJ, 613, 109
Hickox, R. C., Jones, C., Forman, W. R., et al. 2009, ApJ, 696, 891
Hickox, R. C., Myers, A. D., Brodwin, M., et al. 2011, ApJ, 731, 117
Ho, L. C. 2009, ApJ, 699, 626
Hopkins, P. F., & Hernquist, L. 2006, ApJS, 166, 1
Hopkins, P. F., & Hernquist, L. 2009, ApJ, 694, 599
Hopkins, P. F., Hernquist, L., & Cox, T. J. 2006a, ApJS, 163, 1
Hopkins, P. F., Hernquist, L., Cox, T. J., & Kereš, D. 2008, ApJS, 175, 356
Hopkins, P. F., Hernquist, L., Cox, T. J., Robertson, B., & Krause, E. 2007a, ApJ, 669, 45
Hopkins, P. F., Hernquist, L., Cox, T. J., et al. 2005, ApJ, 630, 705
Hopkins, P. F., Hernquist, L., Cox, T. J., et al. 2006b, ApJ, 639, 700
Hopkins, P. F., Hickox, R., Quataert, E., & Hernquist, L. 2009, MNRAS, 398, 333
Hopkins, P. F., & Quataert, E. 2010, MNRAS, 407, 1529
Hopkins, P. F., Richards, G. T., & Hernquist, L. 2007b, ApJ, 654, 731
Hu, J. 2008, MNRAS, 386, 2242
Jahnke, K., & Macciò, A. V. 2011, ApJ, 734, 92
Jiang, L., Fan, X., Bian, F., et al. 2009, AJ, 138, 305
Jiang, L., Fan, X., Vestergaard, M., et al. 2007, AJ, 134, 1150
Jiang, Y.-F., Greene, J. E., Ho, L. C., Xiao, T., & Barth, A. J. 2011, ApJ, 742, 68
Johansson, P. H., Naab, T., & Burkert, A. 2009, ApJ, 690, 802
Kaspi, S., Maoz, D., Netzer, H., et al. 2005, ApJ, 629, 61
Kauffmann, G., & Haehnelt, M. 2000, MNRAS, 311, 576
Kauffmann, G., & Heckman, T. M. 2009, MNRAS, 397, 135
Kauffmann, G., Heckman, T. M., Tremonti, C., et al. 2003, MNRAS, 346, 1055
Kelly, B. C., & Bechtold, J. 2007, ApJS, 168, 1
Kelly, B. C., Bechtold, J., Trump, J. R., Vestergaard, M., & Siemiginowska, A. 2008, ApJS, 176, 355
Kelly, B. C., & Merloni, A. 2012, AdAst, 2012, 970858
Kelly, B. C., Vestergaard, M., & Fan, X. 2009, ApJ, 692, 1388
Kelly, B. C., Vestergaard, M., Fan, X., et al. 2010, ApJ, 719, 1315 (K10)
King, A. R., & Pringle, J. E. 2007, MNRAS, 377, L25
Kocevski, D. D., Faber, S. M., Mozena, M., et al. 2012, ApJ, 744, 148
Kollmeier, J. A., Onken, C. A., Kochanek, C. S., et al. 2006, ApJ, 648, 128
Kormendy, J., Bender, R., & Cornell, M. E. 2011, Natur, 469, 374
Kormendy, J., & Richstone, D. 1995, ARA&A, 33, 581
Koss, M., Mushotzky, R., Veilleux, S., & Winter, L. 2010, ApJL, 716, 125
Kotilainen, J. K., Falomo, R., Labita, M., Treves, A., & Uslenghi, M. 2007, ApJ, 660, 1039
Krolik, J. H. 2001, ApJ, 551, 72
Kurk, J. D., Walter, F., Fan, X., et al. 2007, ApJ, 669, 32
Labita, M., Decarli, R., Treves, A., & Falomo, R. 2009a, MNRAS, 396, 1537
Labita, M., Decarli, R., Treves, A., & Falomo, R. 2009b, MNRAS, 399, 2099
Lapi, A., Shankar, F., Mao, J., et al. 2006, ApJ, 650, 42
Lauer, T. R., Tremaine, S., Richstone, D., & Faber, S. M. 2007, ApJ, 670, 249
Li, Y.-R., Ho, L. C., & Wang, J.-M. 2011, ApJ, 742, 33
Lilly, S. J., Le Fèvre, O., Renzini, A., et al. 2007, ApJS, 172, 70
Liu, X., Shen, Y., & Strauss, M. A. 2012, ApJ, 745, 94
Lodato, G., & Natarajan, P. 2007, MNRAS, 377, L64
Lotz, J. M., Jonsson, P., Cox, T. J., & Primack, J. R. 2010, MNRAS, 404, 575
Madau, P., & Rees, M. J. 2001, ApJL, 551, 27
Magorrian, J., Tremaine, S., Richstone, D., et al. 1998, AJ, 115, 2285
Mandelbaum, R., Li, C., Kauffmann, G., & White, S. D. M. 2009, MNRAS, 393, 377
Marconi, A., Axon, D. J., Maiolino, R., et al. 2008, ApJ, 678, 693
Marconi, A., & Hunt, L. K. 2003, ApJL, 589, 21
Marconi, A., Risaliti, G., Gilli, R., et al. 2004, MNRAS, 351, 169
McConnell, N. J., Ma, C.-P., Gebhardt, K., et al. 2011, Natur, 480, 215
McLure, R. J., & Dunlop, J. S. 2001, MNRAS, 327, 199
McLure, R. J., & Dunlop, J. S. 2002, MNRAS, 331, 795
McLure, R. J., & Dunlop, J. S. 2004, MNRAS, 352, 1390
McLure, R. J., & Jarvis, M. J. 2002, MNRAS, 337, 109
Merloni, A. 2004, MNRAS, 353, 1035
Merloni, A., Bongiorno, A., Bolzonella, M., et al. 2010, ApJ, 708, 137
Merloni, A., & Heinz, S. 2008, MNRAS, 388, 1011
Merritt, D., & Ferrarese, L. 2001, ApJ, 547, 140
Monaco, P., Fontanot, F., & Taffoni, G. 2007, MNRAS, 375, 1189
Mortlock, D. J., Warren, S. J., Venemans, B. P., et al. 2011, Natur, 474, 616
Murray, N., Quataert, E., & Thompson, T. A. 2005, ApJ, 618, 569
Myers, A. D., Brunner, R. J., Nichol, R. C., et al. 2007, ApJ, 658, 85
Nandra, K., Georgakakis, A., Willmer, C. N. A., et al. 2007, ApJL, 660, 11
Natarajan, P., & Treister, E. 2009, MNRAS, 393, 838
Natarajan, P., & Volonteri, M. 2012, MNRAS, 422, 2051
Netzer, H., Lira, P., Trakhtenbrot, B., Shemmer, O., & Cury, I. 2007, ApJ, 671, 1256
Nobuta, K., Akiyama, M., Ueda, Y., et al. 2012, ApJ, 761, 21
Norman, C., & Scoville, N. 1988, ApJ, 332, 124
Onken, C. A., Ferrarese, L., Merritt, D., et al. 2004, ApJ, 615, 645
Park, D., Kelly, B. C., Woo, J.-H., & Treu, T. 2012a, ApJS, 203, 14
Park, D., Woo, J.-H., Treu, T., et al. 2012b, ApJ, 747, 30
Peng, C. Y. 2007, ApJ, 671, 1098
Peng, C. Y., Impey, C. D., Rix, H.-W., et al. 2006, ApJ, 649, 616
Peterson, B. M., Ferrarese, L., Gilbert, K. M., et al. 2004, ApJ, 613, 682
Pierce, C. M., Lotz, J. M., Laird, E. S., et al. 2007, ApJL, 660, 19
Porciani, C., Magliocchetti, M., & Norberg, P. 2004, MNRAS, 355, 1010
Portinari, L., Kotilainen, J., Falomo, R., & Decarli, R. 2012, MNRAS, 420, 732
Pović, M., Sánchez-Portal, M., Pérez García, A. M., et al. 2012, A&A, 541, A118
Rafiee, A., & Hall, P. B. 2011a, MNRAS, 415, 2932
Rafiee, A., & Hall, P. B. 2011b, ApJS, 194, 42
Richards, G. T., Croom, S. M., Anderson, S. F., et al. 2005, MNRAS, 360, 839
Richards, G. T., Kruczek, N. E., Gallagher, S. C., et al. 2011, AJ, 141, 167
Richards, G. T., Strauss, M. A., Fan, X., et al. 2006, AJ, 131, 2766
Rigby, E. E., Best, P. N., Brookes, M. H., et al. 2011, MNRAS, 416, 1900
Roeder, K., & Wasserman, L. 1997, JASA, 92, 894
Ross, N. P., Shen, Y., Strauss, M. A., et al. 2009, ApJ, 697, 1634
Rubin, D. B. 1981, J. Educational Statistics, 6, 377
Rubin, D. B. 1984, AnSta, 12, 1151
Saglia, R. P., Tonry, J. L., Bender, R., et al. 2012, ApJ, 746, 128
Salucci, P., Szuszkiewicz, E., Monaco, P., & Danese, L. 1999, MNRAS, 307, 637
Sanders, D. B., & Mirabel, I. F. 1996, ARA&A, 34, 749
Sanders, D. B., Soifer, B. T., Elias, J. H., et al. 1988, ApJ, 325, 74
Schawinski, K., Dowlin, N., Thomas, D., Urry, C. M., & Edmondson, E. 2010, ApJL, 714, 108
Schawinski, K., Treister, E., Urry, C. M., et al. 2011, ApJL, 727, 31
Schawinski, K., Virani, S., Simmons, B., et al. 2009, ApJL, 692, 19
Schulze, A., & Wisotzki, L. 2010, A&A, 516, A87
Schulze, A., & Wisotzki, L. 2011, A&A, 535, A87
Serber, W., Bahcall, N., Ménard, B., & Richards, G. 2006, ApJ, 643, 68
Sesana, A., Volonteri, M., & Haardt, F. 2007, MNRAS, 377, 1711
Shankar, F., Bernardi, M., & Haiman, Z. 2009a, ApJ, 694, 867
Shankar, F., Crocce, M., Miralda-Escudé, J., Fosalba, P., & Weinberg, D. H. 2010, ApJ, 718, 231
Shankar, F., Salucci, P., Granato, G. L., De Zotti, G., & Danese, L. 2004, MNRAS, 354, 1020
Shankar, F., Weinberg, D. H., & Miralda-Escudé, J. 2009b, ApJ, 690, 20
Shankar, F., Weinberg, D. H., & Miralda-Escudé, J. 2013, MNRAS, 428, 421
Shen, Y. 2009, ApJ, 704, 89
Shen, Y., Greene, J. E., Strauss, M. A., Richards, G. T., & Schneider, D. P. 2008, ApJ, 680, 169
Shen, Y., Hennawi, J. F., Shankar, F., et al. 2010, ApJ, 719, 1693
Shen, Y., & Kelly, B. C. 2010, ApJ, 713, 41
Shen, Y., & Kelly, B. C. 2012, ApJ, 746, 169 (Paper I)
Shen, Y., & Liu, X. 2012, ApJ, 753, 125
Shen, Y., Mulchaey, J. S., Raychaudhury, S., Rasmussen, J., & Ponman, T. J. 2007a, ApJL, 654, 115
Shen, Y., Richards, G. T., Strauss, M. A., et al. 2011, ApJS, 194, 45

Shen, Y., Strauss, M. A., Oguri, M., et al. 2007b, AJ, 133, 2222
Shen, Y., Strauss, M. A., Ross, N. P., et al. 2009, ApJ, 697, 1656
Shlosman, I., Frank, J., & Begelman, M. C. 1989, Natur, 338, 45
Sijacki, D., Springel, V., Di Matteo, T., & Hernquist, L. 2007, MNRAS, 380, 877
Sijacki, D., Springel, V., & Haehnelt, M. G. 2009, MNRAS, 400, 100
Silk, J., & Rees, M. J. 1998, A&A, 331, L1
Silverman, J. D., Green, P. J., Barkhouse, W. A., et al. 2008, ApJ, 679, 118
Silverman, J. D., Kampczyk, P., Jahnke, K., et al. 2011, ApJ, 743, 2
Silverman, J. D., Lamareille, F., Maier, C., et al. 2009, ApJ, 696, 396
Soltan, A. 1982, MNRAS, 200, 115
Somerville, R. S., Hopkins, P. F., Cox, T. J., Robertson, B. E., & Hernquist, L. 2008, MNRAS, 391, 481
Springel, V., Di Matteo, T., & Hernquist, L. 2005, ApJL, 620, 79
Steffen, A. T., Barger, A. J., Cowie, L. L., Mushotzky, R. F., & Yang, Y. 2003, ApJL, 596, 23
Steinhardt, C. L. 2011, ApJ, 738, 110
Steinhardt, C. L., & Elvis, M. 2010a, MNRAS, 402, 2637
Steinhardt, C. L., & Elvis, M. 2010b, MNRAS, 406, L1
Sulentic, J. W., Repetto, P., Stirpe, G. M., et al. 2006, A&A, 456, 929
Tamura, N., Ohta, K., & Ueda, Y. 2006, MNRAS, 365, 134
Tanaka, T., & Haiman, Z. 2009, ApJ, 696, 1798
Trakhtenbrot, B., Netzer, H., Lira, P., & Shemmer, O. 2011, ApJ, 730, 7
Treister, E., Schawinski, K., Urry, C. M., & Simmons, B. D. 2012, ApJL, 758, 39
Tremaine, S., Gebhardt, K., Bender, R., et al. 2002, ApJ, 574, 740
Treu, T., Malkan, M. A., & Blandford, R. D. 2004, ApJL, 615, 97
Treu, T., Woo, J.-H., Malkan, M. A., & Blandford, R. D. 2007, ApJ, 667, 117
Trump, J. R., Impey, C. D., Kelly, B. C., et al. 2009, ApJ, 700, 49
Trump, J. R., Impey, C. D., Kelly, B. C., et al. 2011, ApJ, 733, 60
Trump, J. R., Impey, C. D., McCarthy, P. J., et al. 2007, ApJS, 172, 383
Tundo, E., Bernardi, M., Hyde, J. B., Sheth, R. K., & Pizzella, A. 2007, ApJ, 663, 53
Ueda, Y., Akiyama, M., Ohta, K., & Miyaji, T. 2003, ApJ, 598, 886
Urry, C. M., & Padovani, P. 1995, PASP, 107, 803
Vasudevan, R. V., & Fabian, A. C. 2007, MNRAS, 381, 1235
Vasudevan, R. V., & Fabian, A. C. 2009, MNRAS, 392, 1124
Vestergaard, M. 2002, ApJ, 571, 733
Vestergaard, M. 2004, ApJ, 601, 676
Vestergaard, M., Fan, X., Tremonti, C. A., Osmer, P. S., & Richards, G. T. 2008, ApJL, 674, 1
Vestergaard, M., & Osmer, P. 2009, ApJ, 699, 800
Vestergaard, M., & Peterson, B. M. 2006, ApJ, 641, 689
Vika, M., Driver, S. P., Graham, A. W., & Liske, J. 2009, MNRAS, 400, 1451
Volonteri, M. 2010, A&ARv, 18, 279
Volonteri, M., & Begelman, M. C. 2010, MNRAS, 409, 1022
Volonteri, M., Lodato, G., & Natarajan, P. 2008, MNRAS, 383, 1079
Wandel, A., Peterson, B. M., & Malkan, M. A. 1999, ApJ, 526, 579
Wang, J.-M., Chen, Y.-M., & Zhang, F. 2006, ApJL, 647, 17
White, M., Martini, P., & Cohn, J. D. 2008, MNRAS, 390, 1179
White, M., Myers, A. D., Ross, N. P., et al. 2012, MNRAS, 424, 933
Willott, C. J., Albert, L., Arzoumanian, D., et al. 2010, AJ, 140, 546
Wolf, C., Wisotzki, L., Borch, A., et al. 2003, A&A, 408, 499
Woo, J.-H., Treu, T., Barth, A. J., et al. 2010, ApJ, 716, 269
Woo, J.-H., Treu, T., Malkan, M. A., & Blandford, R. D. 2008, ApJ, 681, 925
Woo, J.-H., & Urry, C. M. 2002, ApJ, 579, 530
Woods, D. F., & Geller, M. J. 2007, AJ, 134, 527
Wuyts, S., Forster Schreiber, N. M., Genzel, R., et al. 2012, ApJ, 753, 25
Wyithe, J. S. B., & Loeb, A. 2003, ApJ, 595, 614
Xue, Y. Q., Brandt, W. N., Luo, B., et al. 2010, ApJ, 720, 368
Younger, J. D., Hopkins, P. F., Cox, T. J., & Hernquist, L. 2008, ApJ, 686, 815
Yu, Q., & Lu, Y. 2004, ApJ, 602, 603
Yu, Q., & Lu, Y. 2008, ApJ, 689, 732
Yu, Q., Lu, Y., & Kauffmann, G. 2005, ApJ, 634, 901
Yu, Q., & Tremaine, S. 2002, MNRAS, 335, 965
Zakamska, N. L., Strauss, M. A., Krolik, J. H., et al. 2006, AJ, 132, 1496